Universidade de Aveiro Departamento de Física
2011

Cristina Schiţco

Propriedades térmicas e eléctricas de nanocompósitos de PVDF/Cu

Thermal and electrical properties of PVDF/Cu nanocomposites

Universidade de Aveiro Departamento de Física
2011

Cristina Schiţco

Propriedades térmicas e eléctricas de nanocompósitos de PVDF/Cu

Thermal and electrical properties of PVDF/Cu nanocomposites

dissertação apresentada à Universidade de Aveiro para cumprimento dos requisitos necessários à obtenção do grau de Mestre em Ciência e Engenharia de Materiais, realizada sob a orientação científica da Doutora Paula Maria Silveirinha Vilarinho, Professor Associado do Departamento de Engenharia de Cerâmica e do Vidro da Universidade de Aveiro e da Doutora Ana Luísa Daniel da Silva, Investigadora Auxiliar do Centro de Investigação em Materiais Cerâmicos e Compósitos (CICECO) da Universidade de Aveiro.

I dedicate this work to my family who has been a constant support throughout my life.

o júri

presidente

Prof. Doutor Maria Margarida Tavares Lopes De Almeida
professora auxiliar do Departamento de Engenharia Cerâmica e do Vidro, da Universidade de Aveiro

Prof. Doutor Carlos Jorge Mariano Miranda Dias
professor auxiliar do Departamento de Ciência dos Materiais, da Universidade Nova de Lisboa

Prof. Doutor Paula Maria Lousada Silveirinha Vilarinho
professora associada do Departamento de Engenharia Cerâmica e do Vidro da Universidade de Aveiro

Doutora Ana Luísa Daniel da Silva
investigadora auxiliar do Laboratório Associado em Materials Cerâmicos e Compósitos, CICECO, da Universidade de Aveiro

agradecimentos

I would like to express my gratitude to
- my superviser Prof. Paula Vilarinho for her precious contribution to my scientific and personal development
- my cosuperviser Ana Luisa for her friendly attitude, constant help and scientific advice
- Prof. Tito Trindade and Ricardo for providing the copper nanowires
- Bruna and Alvaro for their unconditional help in experimental work
- Pedro for his valuable help in performing thermal conductivity measurements
- all my research colleagues from Electroceramics group for providing an excellent work environment and scientific advices
- my friend Christian for constant moral support
- Erasmus Mundus programme for providing a great academical and personal educational experience
- my family for their unconditional love and moral support, without which this thesis would not have been possible first of all

palavras-chave

poli (fluoreto de vinilideno), nanopartículas de cobre, propriedades térmicas, propriedades dielétricas.

resumo

Neste trabalho foram preparados filmes nanocompósitos de poli (fluoreto de vinilideno) (PVDF) com nanoesferas e nanofios de cobre. Foram estudadas a morfologia, propriedades dieléctricas e condutividade térmica. O papel da dimensionalidade do enchimento (*fillers*) foi avaliado e discutido.

As nanopartículas esféricas ou nanofios de cobre foram incorporados na matriz polimérica até 0,30% em peso, através da conformação de soluções de dimetilformamida (DMF). Os filmes obtidos mostraram-se porosos quando analisados por microscopia electrónica de varrimento (SEM). A porosidade dos filmes foi eliminada por uma etapa de prensagem a quente.

Espectroscopias de Infravermelho (FTIR) e Raman indicaram a formação da fase γ na matriz polimérica para ambos os tipos de *fillers*, nano esferas e nanofios de cobre.

A presença de Cu na matriz do polímero só foi detectada por espectroscopia UV-VIS e Difracção de raios X (XRD) para altos teores de nanopartículas.

A cristalização do polímero não foi significativamente afectada no caso da carga com nanoesferas de Cu. Contudo, foi observada um aumento do grau de cristalização (ΔX_c) com a carga para os nanofios de Cu (amostras prensadas).

Medições da resposta eléctrica e térmica revelaram uma melhoria significativa da constante dieléctrica e da condutividade térmica em comparação com PVDF puro. Quando a carga de nanopartículas de Cu equivale a 0,30%, a constante dieléctrica e a condutividade térmica dos nanocompósitos com partículas esféricas é de aproximadamente 20 a 10^3 Hz e 0,39 W/mK, respectivamente. No entanto, e particularmente interessante, este efeito é mais evidente para os nanocompósitos com nanofios de Cu, para os quais a constante dieléctrica e a condutividade térmica atingem valores de 24,4 a 10^3 Hz e 0,45 W/mK, respectivamente. Estes resultados, até agora não reportados na literatura, são de relevância para futuras aplicações de PVDF em dispositivos controladores de stress eléctrico, de blindagem electromagnética e de alta capacidade de armazenamento de energia eléctrica.

keywords poly(vinylidene fluoride), copper nanoparticles, thermal properties, dielectrical properties.

abstract

Poly(vinylidene fluoride) (PVDF) nanocomposites films with spherical and 1 Dimension (1D) copper nanoparticles as fillers were prepared; the morphology, dielectric properties, and thermal conductivity were studied. The role of dimensionality of the fillers was assessed and discussed.

Spherical or nanowires copper nanoparticles were incorporated into the polymeric matrix up to 0.30 wt % via solution casting from dimethylformamide DMF, which acts as a good solvent for PVDF. The obtained films were shown to be porous when investigated by Scanning Electron Microscopy (SEM). The porosity of the films was eliminated by a hot pressing step.

Fourier transform infrared (FTIR) and Raman spectroscopy investigations indicated the formation of γ-phase in the pure polymer as for polymer matrix for both spherical and nanowires copper nanoparticles loading.

The presence of Cu in the polymer matrix was only detected for high nanoparticles contents by UV-Vis spectroscopy and X Ray Diffraction (XRD).

The crystallization of the polymer was not significantly affected in the case of Cu spheres nanoparticles loading. For Cu nanowires, an increase of the degree of crystallization (ΔX_c) with Cu loading was observed (pressed samples).

The dielectric and thermal conductivity measurements showed a significant improvement of the dielectric constant and thermal conductivity compared to pure PVDF. When the loading of Cu nanoparticles equals to 0.30%, the dielectric constant and thermal conductivity of the nanocomposites incorporating spherical particles is ~20 at 10^3 Hz and 0.39 W/mK, respectively. However and particularly interesting this effect is more noticeable for Cu nanowires nanocomposites for which the dielectric constant and the thermal conductivity reached values of 24.4 at 10^3 Hz and 0.45 W/mK, respectively. These results, until now not reported in the literature, have a unique relevance for future applications of PVDF as electric stress control, electromagnetic shielding and high storage capability of the electric energy devices.

Index

List of Figures

List of Tables

List of symbols

d_{ij}	Piezoelectric charge constant
α, β, γ, δ or II, I, III, II_p respectively	Crystalline modifications of poly-1,1-difluoroethene (PVDF)
T	Trans
G	Gauche
T_g	Glass transition temperature
T_m	Melting temperature
$tan\delta_e$	Dielectric loss
P_r	Remnant polarization
T_c	Curie temperature
E_c	Coercive field
p_i	Pyroelectric coefficient
D	Electric displacement
T	Applied stress
S	Strain
E	Applied electric filed
ε	Dielectric permittivity
ε’	Real part of dielectric permittivity
ε’’	Imaginary part of dielectric permittivity
ε_{eff}	Effective dielectric constant
Φ_{QC}	Volume fraction of fillers
Φ_C	Volume fraction of fillers at percolation threshold
s	Critical exponent
θ	Bragg angle
d	Spacing between atomic planes
ΔX_c	The degree of crystallinity for a sample
ΔH_f	The melting enthalpy for a sample
ΔH_{100}	The melting enthalpy for a 100% crystalline sample

1. Introduction: problem formulation

Polymer composites with high dielectric constant and high thermal conductivity are highly desirable for applications such as electric stress control, electromagnetic shielding, and higher energy storage capability like supercapacitors [1].

Polymer matrix holds advantages over ceramic materials through good processability and physicochemical properties (Table 1.1). The highest advantage of polymers as seen in Table 1.1 is based on the very low density and high ductility of polymers compared to ceramics. Thus cheap, light components with complex profiles can be created. On the other hand, polymers have low dielectric constant and thermal conductivity.

Table 1.1 General comparision of materials properties.

Property	**Ceramic**	**Polymer**	**Metal**
Density	Low	Very low	High
Hardness	Very high	Very low	Low
Elastic modulus	Very high	Low	High
Ductility	Low	High	High
Electrical conductivity	Depends on material	Low	High
Thermal conductivity	Depends on material	Very Low	High
Dielectric constant	Very high	Low	-

For example in electric stress control materials, dielectric constant values ranging around 20 are requested[50], while the values of dielectric constant for polymers are in the range of 2-12[7].Composites with high dielectric constant inclusions are an efficient approach to increase the dielectric response of the polymer. Within high dielectric constant fillers lay the ceramic particles of the perovskite type group, such as barium titanate ($BaTiO_3$) or lead zirconate titanate ($PbZr_{1-x}Ti_xO_3$), some of the materials with the highest dielectric constants. However high ceramic filler loadings are usually needed to achieve high dielectric constant what often results in the deterioration of the mechanical and other electrical properties of the matrix[1].

Lately, based on the Maxwell-Wagner-Sillars or interfacial polarization theory[49], a number of researchers [2-6] suggested the use of metallic fillers to increase the polymer dielectric

constant. Designated by Boundary Layer Capacitor Effect (BLCE) it is based on the increase of the polarization by space charge polarization between two materials with different resistivity. When metallic nanoparticles are incorporated into the polymer matrix, a large number of equivalent elementary capacitors are formed. Metallic particles or clusters are isolated by thin dielectric insulating layers. Therefore, when an external electric field is applied, and according to Maxwell-Wagner-Sillars theory, charge depletion layers are created and the dielectric constant of the nanocomposite is enhanced from the build-ups of charge [2]. Therefore, when a critical volume fraction of conductive components is added to an insulator matrix, there is a major increase in the dielectric constant. This behavior is common for conductor (metal) / insulator (polymer) when percolation threshold is reached [3]. The critical volume fraction of conductive components depends on processing parameters as of size and shape of the filler particle[3].

Obviously, nanoparticles are preferred for metal/polymer composite since the volume fraction of conductive components can be lowered by reducing the filler dimensions whereas the flexibility of the polymer matrix is retained.

On the other hand, fast cooling (high thermal conductivity) is essential for microelectronics and high-voltage industry[1]. Materials with very high thermal conductivity for supercapacitors as nearly around 200 W/mK[51] are requested. An effective approach to increase the cooling rate of dielectrics to be used in supercapacitors, high storage energy devices, etc., is to use as fillers materials with high thermal conductivity as metals (Table 1.1). Among metals, Cu has the second highest thermal conductivity (401 W/mK) after Ag (429 W/mK)[7] and in addition is a very low cost metal.

Within this context, the purpose of this work is to prepare polymer composites with high dielectric constant and high thermal conductivity using low-cost materials. The followed strategy included the fabrication of PVDF polymer films embedded with Cu nanoparticles of different dimensionality (spherical and nanowires shape). The systematic and detailed characterization of the structure, microstructure, and physical properties of the prepared composites, allowed the identification of the role of fillers particle dimensionality on the structural and physical properties of the composite. The relationship between the filler content and dimensionality with the thermal and dielectric response of PVDF / Cu nanoparticles composites was established.

2. Literature review

This chapter presents and briefly discusses the known data on the polymer used as a matrix, polyvinylidene fluoride (PVDF), and metals used as fillers (Cu nanoparticles) in this work.

2.1 PVDF

Although PVDF exhibits a variety of interesting mechanical and chemical properties, it is best known for its piezoelectricity which is the largest among synthetic polymers[8]. PVDF is the first ferroelectric polymer known[8,10], making it unique among many inorganic and organic materials.

2.1.1 Nomenclature. History

Polyvinylidene fluoride or PVDF is a non-reactive, thermoplastic polymer.

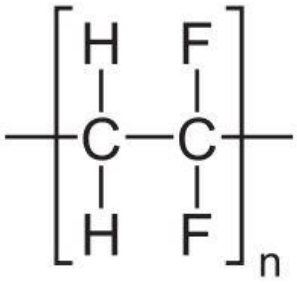

Figure 2.1 Polyvinylidene fluoride structure[9].

The polymer is known under IUPAC name of poly-1,1-difluoroethene. Other names such as: polyvinylidene diflouride, KYNAR, HYLAR, SOLEF, SYGEF, are also referred in the literature[9].

Investigations on piezoelectric polymers date back to 1920. Small piezoelectric effect was noticed in rubber, celluloid, and in biological polymers like protein keratin.

Later on, in 1968, piezoelectric activity was reported in commercially available polymers like polystyrene, polypropylene, and poly(methyl methacrylate). The largest breakthrough came in 1969 when Kawai et al discovered that stretched and poled PVDF exhibits some of

the largest piezoelectric activity among polymers (d_{33} = 6-7 pC/N): 10 times larger than that observed in any other polymer[10].

The discovery of pyroelectric effect in PVDF followed in 1971 and originated a variety of important new applications for PVDF. During the 70's the research was extended to copolymers of vinylidene fluoride (VDF) and fluorinated vinyl monomers: vinyl fluoride (VF), trifluotoethylene (TrFE) and tetraflouroethylene (TrFE)[10].

2.1.2 Structure. Crystalline phases

PVDF has a simple chemical formula: -CH_2-CF_2-. The chemical formula is intermediate between –CH_2-CH_2- (PE-polyethylene) and CF_2-CF_2- (PTFE-polytetrafluoroethylene). This simplicity of the chemical formula gives both high flexibility (as seen in PE) and some stereochemical constraint (as seen in PTFE). The monomeric unit has the directionality of CH_2 (head)-CF_2 (tail).

In PVDF, CH_2 group dilutes CF_2-CF_2 interactions, because it is located at an intermediate position between CF_2 groups. PVDF can take various conformations; a conformation is understood as the order that arises from the rotation of molecules about the single bonds. Depending on the conformation taken, the existence of both trans (synonymous with an antiperiplanar angle alignment of groups attached to adjacent atoms, from -150° to 180°:T or T^-, 150° to 180°:T or T^+)[52,53] and gauche (synonymous with a synclinal alignment of groups attached to adjacent atoms, from -30° to -90°:$\bar{G}$ or G^-, 30° to 90°:G or G^+)[53,54] isomers are possible. This is the main reason why PVDF can take a variety of molecular conformation as well as crystal structures.

PVDF can take at least three different types of molecular conformations: alpha α TGT$\bar{G}$, beta β TTTT, and gama γ TTTGTTT$\bar{G}$. Concerning the packing modes of these molecular chains into the unit cell four types of crystalline modifications exists: α, β, γ, and δ (correspondingly forms II, I, III, and IV) (or polar form II, IIp).

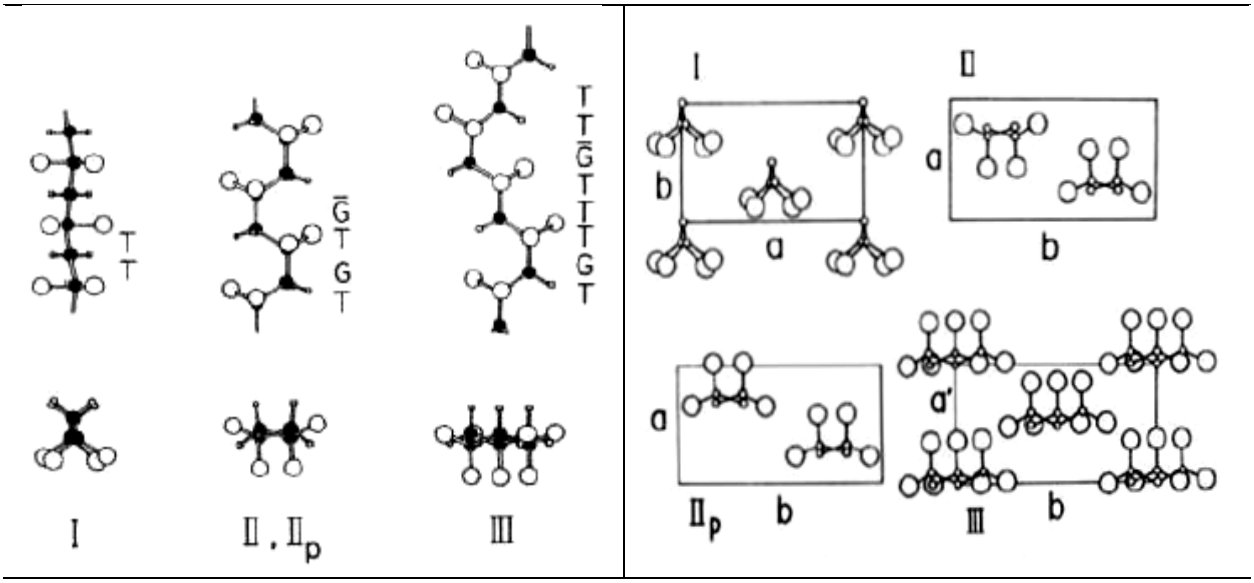

Figure 2.2 Molecular structure (left) and crystal structure (right) of four crystalline modifications of PVDF[8].

A brief summary of PVDF conformations and correspondent synthesis process is given in the Table 2.1.

Table 2.1 PVDF crystalline modifications (modified from Ref. 11).

Crystalline modification	Conformation	Preparation	Polarity
α (Form II)	TGTḠ)	Solution deposition	Non-polar
β (Form I)	TTTT	Stretching (oriented)	Polar
γ (Form III)	$T_3GT_3\bar{G}$	Solution deposition (unordered) Annealing near the melting point (ordered)	Polar
δ (Form II_p)	Similar to α, except other chain is rotated making it electrically active	Poling in electrical field	Polar

2.1.2.1 α - phase

Most common polymorph of PVDF is α phase. Each chain conformation possesses a net dipole moment which originates from -CF_2 bond (Figure 2.3). Each component of the net

dipole moment is perpendicular to the polymer chain. Because the dipole components normal to the chain are antiparallel, they cancel each other rendering a non-polar form to the α-phase.

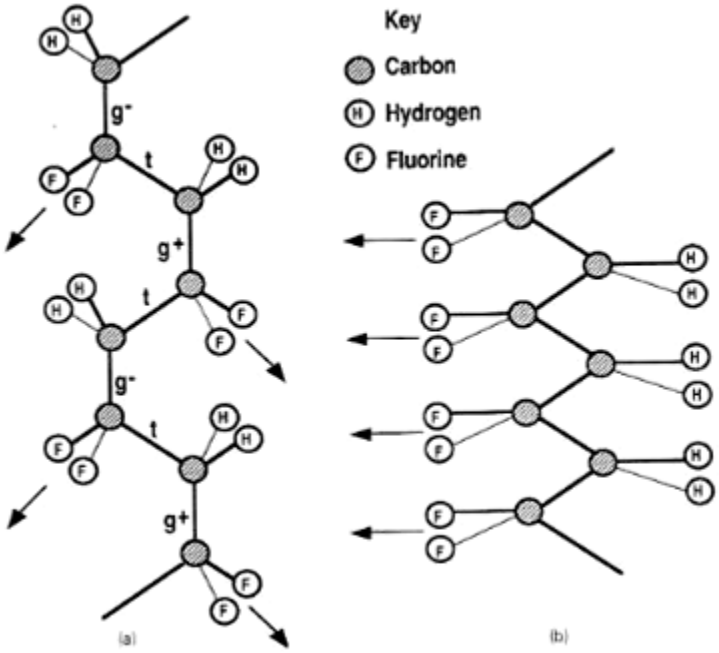

Figure 2.3 Scheme of two most common crystalline modifications of PVDF: a) α-phase; b) β-phase. Arrows indicate the direction of $–CF_2$ dipole moment normal to the carbon backbone[10].

2.1.2.2 β - phase

The β-phase is obtained when α-phase is mechanical stretched or rolled at elevated temperatures. β-phase has all-trans conformation. At a microscopic level all dipoles are normal to the chain axes, thus each crystallite exhibits a net dipole and is piezoelectric as shown in Figure 2.3. However, at a macroscopic level there is zero polarization due to a random orientation of the crystallites. When applying an electric field PVDF becomes piezoelectric producing a net polarization. The crystallites are oriented in the direction of the field, a process known as poling.

2.1.2.3 γ - phase

For many years this polymorph could not be obtained in oriented form because it transforms rapidly into β-phase under mechanical deformation[12].

This structure possesses polar unit cells, but the dipole moments are smaller than in β-phase[8].

2.1.3 Synthesis. Processing

PVDF if formed by linking together VDF (1,1-difluoroethylene) molecules. VDF monomer ($CH_2=CF_2$) is a stable gas at normal temperatures and pressures. Commercially the monomer is produced by pyrolysis adding catalysts. The precursor used is trifluoroethane following the equation:

$$CF_3CH_3 \xrightarrow{\text{heat}} CH_2=CF_2 + HF \quad (1)$$

Industrially the polymerization of the VDF is a free-radical polymerization reaction in suspension or emulsion, using water as reaction medium. The reaction is carried out at 20-60 °C and pressures up to 60 MPa[10].

Laboratory scale the reaction is carried out in liquid phase using alcoholic potassium hydroxide and halogen-substituted ethane[10].

$$CHF_2CH_2Br + KOH(\text{alcoholic}) \xrightarrow{\text{heat}} CH_2=CF_2 + KBr + H_2O \quad (2)$$

Figure 2.4 summarizes the interrelation between these phases which can be transformed within each other by changing some external condition during or post synthesis.

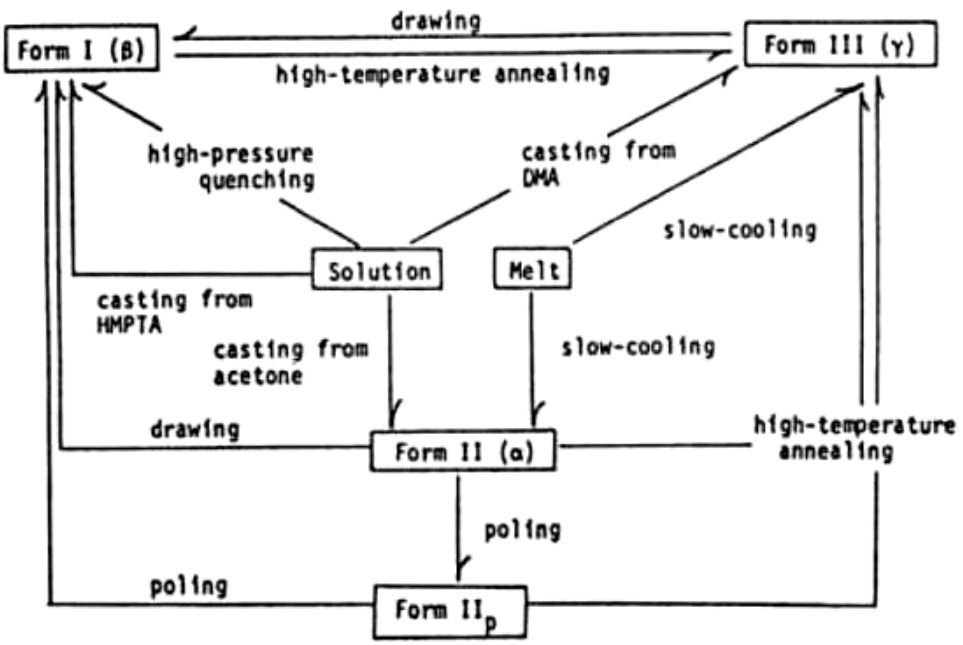

Figure 2.4 Interconversion between the crystal of PVDF by changing an external synthesis condition[8].

2.1.3.1 Synthesis of α - phase

Crystal form II (α-phase) is easier to prepare than the other crystalline forms. The polymer melt is cooled down to room temperature at a normal rate, giving the unoriented form II. When the melt is cooled down slowly, forms I and III may also result in the process. On the other hand, an extremely fast cooling rate (ultrafast quenching) results solely in form I. To obtain α phase at room temperature, casting from acetone method is usually employed[8]. The polymer sample obtained by this method is also unoriented as the one prepared by melting, although some preferential orientation occurs in the film plane.

Oriented form II can be obtained either by drawing of unoriented sample at high temperature (above 130-160 ^{o}C) or by direct stretching of the melt at room temperature during crystallization of uniaxially oriented polymer form II.

2.1.3.2 Synthesis of β - phase

β phase can be obtained following the roots:

- Stretching at room temperature the unoriented form II, obtained by cooling the melt at a normal rate (10-20^{o}C/min or higher).

- Stretching of form III results in uniaxially oriented β phase polymers.
- Rolling form II at room temperature gives uniaxially oriented β phase polymers.
- Casting from (hexamethylphosphorictriamide) HMPTA by precipitating (dimethylacetamide) DMA solution into acetic acid aqueous solution.
- Rapid quenching of the molten sample into a liquid nitrogen reservoir (unoriented form).
- Annealing at high pressure and high temperature (ca. 400 MPa, 570 K) of the polymer sample.
- Quenching the melt at high pressure[8].

2.1.3.3 Synthesis of γ - phase

Preparation of unoriented form III can be done in the following ways:

- Casting from DMA or dimethylformamide (DMF) at 60 ^{o}C.
- Isothermal crystallization of the molten sample at temperatures below the melting point.
- High pressure and high temperature crystallization.
- High temperature annealing of the crystalline form II gives form III. This transformation occurs under special conditions explained in detail by Lovinger[11].

Oriented form III is difficult to obtain by simple stretching of the solution-cast form III, because it changes easily to form I by drawing.

2.1.4 Physical, electrical, mechanical, and thermal properties

PVDF is a rubbery material with T_g bellow room temperature: -40 °C (T_g - glass transition temperature is the temperature bellow which the polymer behaves in a brittle manner and above it: rubber-like). As most of semicrystalline polymers, PVDF crystallizes in spherulites comprised of crystalline lamellae. The melting point is T_m = 175 °C (Table 2.2), but it depends on lamellae thickness and on crystalline modifications[13]. As it can be seen from Table 2.2, PVDF has a rather low melting temperature compared to other materials, which is a disadvantage for industrial applications.

Thermal conductivity of PVDF is lower than of ceramics due to its loose molecular structure. Values of thermal conductivity of 0.55 W/mK to the draw direction and 0.125 W/mK for the transverse direction have been reported[10], being the lowest compared to metals,

ceramics and some nonmetallic solids like graphene (Tab. 2.2). A very low thermal conductivity as explained earlier presents a big disadvantage for microelectronic applications. On the other hand, metals present a high value of thermal conductivity (in the range of 10^2 W/mK).

The value of Young's modulus for PVDF is typically 1.9-2.0 GPa[10]. Among other polymers, like Teflon (Tab. 2.2), PVDF displays a reasonable elastic modulus, but still much lower than other materials.

Table 2.2 Physical, thermal, electrical, and mechanical properties of some materials including PVDF. RT stands for room temperature.

Material		Melting point (°C)	Thermal conductivity$_{RT}$ (W/mK)	Dielectric constant$_{RT}$	Young's modulus (GPa)
Nonmetallic solids	Graphene	>3600 (reported for graphite)	4840-5300[56]	2.5-3 (reported for carbon black)[58]	500[57]
Metals	Silver	962[7]	429[7]	-	72.4[7]
	Copper	1083[7]	401[7]	-	117.2[7]
Ceramics	BT ($BaTiO_3$)	1625[7]	1.3-6[47]	a-axis: 5000[48] c-axis: 250[48]	67[60]
	PZT($PbZr_{1-x}Ti_xO_3$)	1348[7]	1.25[61]	1700[59]	49-63[59]
Polymers	PVDF	175[10]	Draw direction: 0.55 [10] Transverse direction: 0.125[10]	7-12[10,44] (1 KHz)	1.9-2.0[10]
	Teflon	327[7]	0.225[7]	2 (1 KHz)	0.4-0.7[7]

Most polymers are insulating materials. PVDF is a nonlinear dielectric, thus the surface charge density (D) increases with the field in a nonlinear manner. The values of dielectric constants vary from 10 to 12 at 1 kHz. These values are much lower than those for piezoelectric ceramics (BT-5000, PZT-1700). This fact is regarded as a disadvantage for applications which require materials with high capacitance.

Dielectric loss ($\tan\delta_e$) shows the amount of electrical energy dissipated into thermal energy and it is an important parameter when designing dielectric applications (such as capacitors, sensors, actuators, transducers, among others). The dielectric loss for PVDF at

room temperature quoted in literature ranges from 0.015 to 0.02 at 1 kHz[10]. PVDF is a lossy dielectric compared with the values of 10^{-4} for some ferroelectric ceramics[10].

2.1.5 Electroactive properties. Definition of Piro, Piezo, and Ferroelectricity

Electroactive polymers are the polymers which exhibit a change in shape and size when stimulated by an electric field.

Ferroelectric materials are differentiated through two main features: i) hysteresis loops of the polarization as a function of the electrical field and reversal of the polarization with the switching field; and ii) the phase transition (Curie temperature - T_c) at which the material changes from ferroelectric to paraelectric, a transition that is usually accompanied by a structural phase transition. The hysteric response of a ferroelectric material is characterized by the remnant polarization P_r, and by coercive field, E_c. P_r is defined as the amount of surface charge density that remains after an electric field is removed and that is caused by the net alignment of dipoles within the crystalline phase of the material. E_c is the electric field at which the polarization passes through zero. For PVDF values of P_r and E_c are in the region of 5 μCm^{-2} and 50 $kVmm^{-1}$ respectively[10]. In case of most known ceramics these values constitute for BT: 26 μCm^{-2} and 10 $kVmm^{-1}$ respectively, and for $PbTiO_3$: 75 μCm^{-2} and 7 $kVmm^{-1}$.[62]

In terms of dielectric response, the relative permittivity (dielectric constant) ε_r quoted for PVDF ranges from 10 to 12 at 1kHz, depending on the phase and manufacturer[10] (Tab. 2.2).

The charge stored on a dielectric has both real and imaginary components caused by resistive leakage or dielectric absorption respectively[10]. The dielectric permittivity is a complex quantity:

$$\varepsilon = \varepsilon' - i\varepsilon''$$

where ε' stands for the real component and ε'' for the imaginary part.

The dielectric loss tangent $\tan\delta_e$ is defined as:

$$tan\delta e = \frac{\varepsilon''}{\varepsilon'}$$

The value of the dielectric loss quantifies the amount of electrical energy dissipated into thermal energy[10].

Piezoelectric materials generate an electric charge in response to a mechanical stress, known as the direct piezoelectric effect. In this case the electric displacement D is proportional to the applied stress A. The converse effect, when an applied electric field E produces a proportional strain S in the material, resulting in either expansion or contraction (depends on field's polarity). For both effects, the proportionality constant is named the piezoelectric charge constant d or strain constant (d_{ij} relates a field along the i axis to the strain in the j direction):

$$d = \frac{D}{A} = \frac{S}{E}$$

The d_{33} coefficient is the most commonly cited of these coefficients and it corresponds for both strain and field along the polar axis[63].

A pyroelectric material generates electric charge when subjected to a change in temperature.

The pyroelectric constant p is quantified as following:

$$p = \frac{\Delta P}{\Delta A}$$

When the temperature of the pyroelectric is altered externally by heat conduction or incident radiation, a change in polarization occurs, resulting in a detectable surface charge. Since polarization is a vector, the pyroelectric coefficient is dependent on the direction measured[63], therefore it is designed as p_i, where i = 1, 2, 3.

2.1.6 Applications

PVDF have many applications that include coatings, automobile, battery, chemical process industry, corrosive waste, food and beverage, fuel handling systems, medical, membranes, pharmaceutical, piping, photovoltaics, semiconductors, among others. But a majority part of PVDF application is related with its piezoelectric and pyroelectric properties. The potential of PVDF to be used as light, rugged, large-area flexible material combined with electroactive properties inspired applications such as sound transducers in air, sound transducer in water, mechanical, biomedical, and pyroelectric applications[8,10]. As real applications can be also mentioned sensors for prosthetics, non-invasive cardio-pulmonary sensors, implantable transducers, thermal imaging systems, etc. For these applications

optimized performance is a requirement. In addition for the most current applications as supercapacitors and high voltage storage devices, besides high polarization good heat dissipation is a necessity.

2.2 PVDF composites

The limitations of PVDF in terms of electric performance that is inferior (see Table 2.2) to the most used electromechanical ceramic perovskite based compositions have been the driving force behind the search for solutions to overcome some of these limitations. A promising approach is the fabrication of composite materials. This following chapter discusses the composite comprising polymeric PVDF phase and non polymeric fillers with emphasis on Metal / PVDF nanocomposites.

2.2.1 Introduction

Composites are natural or engineered materials made from at least two constituents with significant different physical or chemical properties in order to enhance the properties of produced composite material. Thus, the properties of the polymer can be greatly enhanced by the use of fillers to form a composite. Fillers can be used to tailor properties like dielectric constant, thermal conductivity, thermal expansion, mechanical properties, etc. As a function of the desired property, fillers can be inorganic powders like ceramics, fibers or metal nanoparticles.

Choosing the correct components to create a composite is not the only criteria followed. Connectivity, symmetry, and the physical and chemical properties of the individual phases are also taken into account. Connectivity (the type of phase coupling) signifies coupling the components in the optimum way. Connectivity is especially important because it controls the electric flux pattern within the composite and its mechanical properties. Depending on the way in which phase connections are made, the physical properties of a composite may change drastically. Each phase may be self-connected in zero, one or three dimension, resulting in 10 diphasic connectivities: 0-0, 1-0, 2-0, 3-0, 1-1, 2-1, 3-1, 2-2, 3-2, 3-3. By convention, in electroactive (change in size and shape when stimulated by an electric field)

composites, the first number refers to the active phase and the second to the inactive phase. The most important connectivities are described below:

- 3-3 connectivity: both phases are connected in all three dimensions. This type of structure is seen in polymer foams and biological substances like wood and coral.
- 3-2 & 3-1 connectivity: the first phase is three-dimensionally connected, while the second phase (the polymer) is one- or two-dimensionally connected within the first phase.
- 1-3 connectivity: consists of one-dimensionally connected phase comprised in a three-dimensional second phase (polymer). An example of this type of connectivity is rod shape PZT covered with epoxy.
- 2-2 connectivity: are also called multilayer structures.
- 0-3 connectivity: is the most common type of connectivity used also in this work and it consists of a three-dimensional polymer matrix loaded with discrete fillers. The most attractive features of the 0-3 design are the versatility of forms in which this composite can be produced, ease of fabrication, and suitability for mass production.

Symmetry is also an important consideration when designing a composite and it involves the crystallographic symmetry of each phase, the phase symmetry after processing, the combined symmetry of the composite, and the environmental influence on the total symmetry[10].

Piezoceramic/PVDF composites were studied to produce piezoelectric devices[10]. Polymer matrix has the advantage of lowering the density of the material and to be easier shaped in the desired profile because of polymer flexibility. For many applications fillers are based on lead titanate ($PbTiO_3$)[10]. Dang Z.-M. and Nan C.-V. suggest the use of Li and Ti co-doped NiO (LTNO) as an alternative for lead perovskite-ceramic, since the last one might release harmful lead gas during sintering[64]. At a loading of 0.4 volume fraction the authors obtain a dielectric constant equal to 80 at 100 Hz[64], which is a relative low enhancement relative to the very high dielectric constant of LTNO itself. Moreover, difficulties are encountered during composites preparation since the ceramics needs to be grinded to fine powder.

Lately, the use of metallic nanoparticles as fillers to increase the dielectric constant and thermal conductivity of the filler attracted great interest. According to Maxwell-Wagner-Sillar interfacial polarization[49], introducing metal nanoparticles large accumulation of charge

carriers are produced which are blocked by the thin insulating boundary of the interface of the two components of the composite. Hence, the nanocomposite behaves like it would be constituted of a large number of equivalent elementary capacitors giving rise to high dielectric constant (Boundary Layer Capacitor Effect[1]).

2.2.2 Metal / PVDF nanocomposites

Several polymer/metal nanocomposites with high dielectric constant are reported in the literature[1-6, 14]. However, there are no systematic studies of the thermal conductivity of the nanocomposites. Table 2.3 presents some of most important data collected from the literature.

According to Table 2.3, the highest dielectric constant (3800 at 10^2 Hz) was reported for PVDF/ $Al_{65}Cu_{23}Fe_{12}$ nanocomposite achieved at 23% volume fraction of conductive particles. Regarding the use of pure metallic nanoparticles as fillers, a value of 2050 at 10^2 Hz was reported for PVDF/Ni nanocomposite at 28% volume fraction of Ni particles. Both these volume fractions correspond to percolation threshold.

Concerning the thermal conductivity, 6.5 Watt•m^{-1}•K^{-1} at room temperature was achieved for PVDF/Ag nanocomposite at a loading of 20 vol.%. On the other hand, Chae D. W. et al. reported a value of 0.38 Watt•m^{-1}•K^{-1} at room temperature for 15.3 vol.% Ag content of PVDF/Ag composite (Table 2.3). There are no studies on thermal conductivity of PVDF nanocomposites containing metal nanoparticles comparable with the ones used in this work.

Table 2.3 Literature results on the dielectric and thermal conductivity properties of PVDF/ nanocomposites with various fillers.

PVDF with	Filler concentration	Phase	Properties				Reference
			Dielectric constant	Increase %	Thermal Conductivity (W/mK)	Increase %	
pure	0	α	8.3 (10^3 Hz)	-	-	-	5
pure	0	β	12.3 (10^3 Hz)	-	-	-	5
pure	0	γ	-	-	-	-	
Ag	90 wt % (15.3 vol%)	α	NR	NR	0.38	81	4
Ag	120 wt %(20 vol%)	NR	120 (10^3 Hz)	1544	6.5	2608	1
Ag	0.02 wt%	α	14.1 (10^3 Hz)	41.1	NR	NR	5
Ag	0.02 wt%	α (30%) & β (70%)	26.7 (10^3 Hz)	54	NR	NR	5
Ni	5* vol%	NR	112 (10^3 Hz)	1020	NR	NR	14
Ni	28* vol%	NR	2050 (10^2 Hz)	20400	NR	NR	2
Ni	20 vol%	NR	68 (10^4 Hz)	548	NR	NR	6
$Al_{65}Cu_{23}Fe_{12}$	23*vol%	NR	3800 (10^2 Hz)	34445	NR	NR	3

NR= not reported
* particle volume fraction corresponding to percolation threshold.

Use of metallic fillers of nano size retains the polymer matrix flexibility and creates a higher number of equivalent elementary capacitors[1]. According to percolation theory the power law dependence of dielectric constant near the percolation threshold is given by:

$$\varepsilon_{eff} \sim (\Phi_C - \Phi_{QC})^{-s} \text{ for } \Phi_{QC} < \Phi_C,$$

where ε_{eff} is the effective dielectric constant, Φ_{QC} is the volume fraction of fillers, Φ_C is the percolation threshold and 's' is the corresponding critical exponent. As seen in Table 2.3, when reaching the particle volume fraction corresponding to percolation threshold the dielectric constant of the nanocomposite is greatly enhanced.

Up to now, there is no information found regarding PVDF/Cu nanocomposites.

2.3 Copper nanoparticles

An effective approach to increase the cooling rate of a PVDF composite is to use as fillers materials with high thermal conductivity as metals. Within metals as stated earlier, Cu has the second highest thermal conductivity (4.01 Watt•cm^{-1}•K^{-1} at 300 K) after Ag (4.29 Watt•cm^{-1}•K^{-1} at 300 K)[7]. Copper nanoparticles, amongst other metal nanoparticles, have attracted interest also because of their catalytic, optical, and electrical properties. However the synthesis of composites with copper faces a big challenge when compared with other metals: copper nanoparticles are highly reactive to air, oxidizing very easily, generating copper oxide layers: Cu_2O, CuO, or mixtures on the surface of Cu nanoparticles[15]. This causes high thermal interface resistance (the measure of an interface's resistance to thermal flow) and it is believed as the main reason why high values of thermal conductivity cannot be easily obtained in polymer/metal nanocomposites[1].

2.3.1 Spherical Copper nanoparticles

Copper nanoparticles with intense surface plasmon resonance band (LSPR) are rather complicated to produce because those are prone to fast oxidation and Cu possesses a low "free-electron character"[16], [31]. Low "free-electron character" means that electronic interband transitions from the valence band to the Fermi level overlap the plasmon resonances up to 600 nm and well-defined plasmon bands in this range cannot be easily obtained[16]. Methods reported for the fabrication of Cu nanoparticles are: UV-light irradiation, pulsed sonoelectrochemical reduction γ-irradiation, chemical or polyol reduction of copper salts grown in reverse micelles[16]. Pileni et al. reported a fair control of size and shape of copper nanoparticles when mixing reverse micelles with a large excess of reducing agents[17].

In the communication of I. P. Pastoriza-Santos et al. a method to prevent fast nanoparticles oxidation was suggested by using DMF (N, N-dimethylformamide) and hydrazine as reducing agent[16].

According to the authors limited oxidation of Cu nanoparticles takes place that results in CuO and Cu_2O formation. The authors argue that an oxide shell with thickness of two atomic layers is sufficient to protect the metal from complete oxidation[18].

2.3.2 Copper nanowires

One-dimensional nanowires have attracted interest because of their novel properties and potential application.(1D) metal nanostructures are expected to play a significant role in fabricating nanoscale electronic, optoelectronic, magnetic devices, as to present physical phenomena such as quantized conductance and size effects[65]. Cu nanowires and nanorods were synthesized by means of electrochemical reactions,vapor-deposition, hard-template-assisted method, colloids, and hydrothermal processes[19, 20]. There is still lack of effective methods for copper nanowires production with precise morphological control. Major synthetic difficulties encountered are polydispersity, short length, nonlinear morphology, and process complexity[42]. The control of reaction conditions like temperature, the nature of complexing agents, the catalyst used, etc. yields nanowires with different shape and dimensionality[42, 65].

Although more resistant to oxidation than Cu nanospheres, the surface of the copper nanowires is also reported to oxidize easily in air to form Cu_2O[19].

3. Experimental methods

This chapter presents the experimental methods used for materials processing and the techniques used for structural, morphological as well as property characterization of PVDF and PVDF/Cu nanocomposites.

3.1 Materials and sample preparation

This section deals with the preparation of PVDF nanocomposites imbedded with spherical or nanowires Cu nanoparticles. The experimental procedure starts with spherical and nanowires Cu nanoparticles synthesis. Further, PVDF film and PVDF/Cu film nanocomposites were prepared. The films were hot pressed to eliminate porosity.

Finally, a summary of experimental procedure is made and sample denomination is explained.

3.1.1 Spherical Copper nanoparticles preparation

The synthesis of Cu nanoparticles was performed following Ref.16. $Cu(CH_3COO)_2.H_2O$ (30 mg, Pancreac) was dissolved in 15 mL dimethylformamide (DMF,Fluka). The solution was heated up to 40 ^oC and after 0.15 mL hydrazine solution (0.1 M, 50-60%, Aldrich) was injected under vigorous stirring. The mixture was stirred for 10 min at 40 ^oC. The temperature was quickly raised up to 60 ^oC and the mixture was stirred for 15 minutes.

Change of color from green to deep purple acts as evidence that the reduction of Cu^{2+} into metallic Cu^o occurred (Figure 3.1).

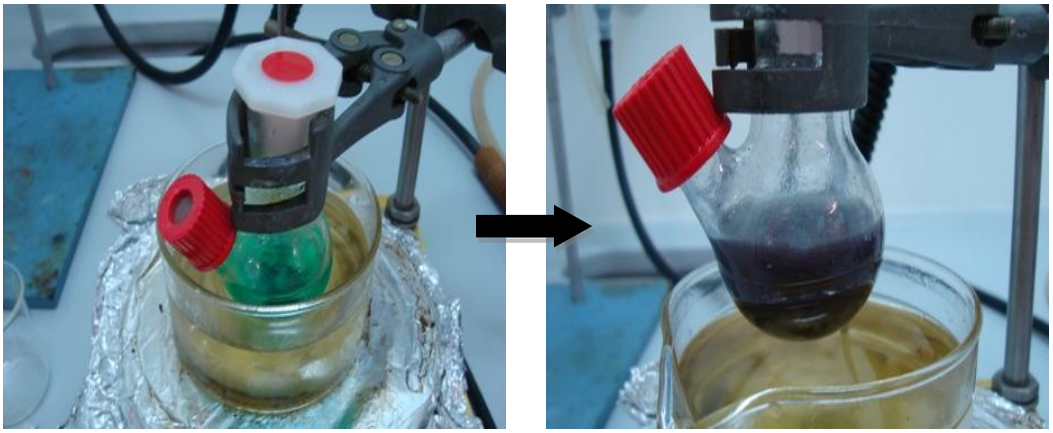

Figure 3.1 Reduction of Cu^{2+} (green) to metallic Cu^{o} (deep purple) (offered with courtesy by Bruna Rosa).

3.1.2 Nanowires Copper particles preparation

A detailed description of Copper nanowires preparation method can be found in Ref. 42. The synthesis of copper nanowires was achieved using low-cost starting chemicals under mild condition (experiment A1 from supporting information of Ref.42)[42].

For each synthesis 20 mL of NaOH (15 M, 98.5%, Acros) and 1.0 mL of $Cu(NO_3)_2 \cdot 3H_2O$ (0.1 M, 99.5%, RPE) were added to a glass reactor with capacity of 50 mL. Consequently 0.15 mL of ethylenediamine (EDA; 99.9%, Aldrich) and 25 µL hydrazine ($N_2H_4 \cdot H_2O$, 50-60%, Sigma-Aldrich) were added, followed by a thorough mixing of the components. The glass reactor was placed in a water bath at 60 ^{o}C for 1 h. Copper products were washed and harvested with centrifugation-redispertion cycles and stored in 15 mL DMF.

The formation of metallic copper is based on the following redox reaction:

$$2Cu^{2+} + N_2H_4 + 4OH^- \rightarrow 2Cu + N_2 + 4H_2O \quad (3)$$

Copper nanowires were investigated with X-ray diffraction (XRD) and UV-Vis spectroscopy. Morphological investigations were carried out with Scanning Electron Microscopy.

3.1.3 PVDF film preparation

PVDF film was obtained by solvent casting method. 2 g of PVDF pellets (Hylar® 9009, Solvay) were dissolved in 10 mL DMF at 60 ^{o}C for 1 h under vigorous stirring. After the pellets dissolved completely, the solution was poured in Petri glass, kept in oven at 60^{o}C during 17 hours in order for the solvent to evaporate.

Figure 3.2 PVDF pellets (left) and PVDF film (right).

3.1.4 Nanocomposite PVDF/Cu film preparation

Regardless of the shape of the particles used, nanospheres or nanowires, the PVDF/Cu preparation method remained the same.

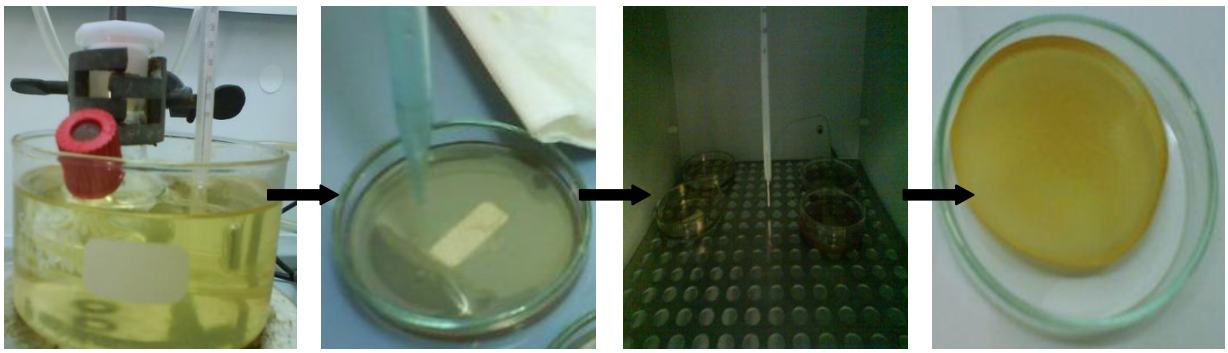

Figure 3.3 PVDF/Cu film nanocomposite preparation. PVDF pellets are dissolved in DMF. After complete dissolution of the polymer, the mixture was spread on Petri glass and dried in the oven at 60 ˚C for 17 hours.

Basically it followed the procedure for pure PVDF preparation except one step. After the polymer pellets were dissolved, a certain calculated volume of Cu particles, either

nanospheres or nanowires, were added to the mixture and stirred vigorously during 30 min at 60^{o}C. The exact amount of reactives added for each sample is described in Table 3.1 and 3.2.

For convenience, the samples were denominated as follows: PVDF, PVDF-0.02CuSph, PVDF-0.05CuSph, PVDF-0.15CuSph, PVDF-0.30CuSph, PVDF-0.02CuNw, PVDF-0.05CuNw, PVDF-0.15CuNw, PVDF-0.30CuNw. The names are explained in Table 4.2 and 4.3. Nw stands for nanowires. Sph stands for nanospheres.

Table 3.1 PVDF/Cu nanospheres sample preparation.

Sample	Cu nanospheres, wt %	V(Cu nanospheres), mL	m(PVDF), g	V(DMF), mL
PVDF	0	0	2	10
PVDF-0.02CuSph	0.02	0.60	2	9.40
PVDF-0.05CuSph	0.05	1.51	2	8.49
PVDF-0.15CuSph	0.15	4.51	2	5.49
PVDF-0.30CuSph	0.30	9.04	2	0.96

Table 3.2 PVDF/Cu nanowires sample preparation.

Sample	Cu nanowires, wt %	V(Cu nanowires), mL	m(PVDF), g	V(DMF), mL
PVDF	0	0	2	10
PVDF-0.02CuNw	0.02	0.47	2	9.53
PVDF-0.05CuNw	0.05	1.18	2	8.82
PVDF-0.15CuNw	0.15	3.54	2	6.46
PVDF-0.30CuNw	0.30	7.08	2	2.92

3.1.5 Hot pressing of the prepared films

The films obtained by solvent casting contain porosity. Porosity influences negatively dielectrical properties of the films. In order to eliminate the porosity, the films were hot pressed. Moreover, a flat surface is required for thermal conductivity measurements.

The samples were pressed according to the procedure:

- The hot plates were inserted in the uniaxial press according to the instructions given. The cooling system and the temperature controller were set. The plates were heated till 150 ˚C.

Figure 3.4 a) Uniaxal press with the hot plates installed b) Temperature controller c) Teflon films.

- The plates were touched and preheated for 2 minutes, without applying pressure.

- The sample was inserted between the plates. The samples were covered on the both side with Teflon films. The films were pressed during 10 min, applying a force of 2 tons.

- The samples were cooled down together with plates until 60 ˚C. The plates cooled down from 150 until 60 ˚C with a rate of 4˚C/min.

3.2 Characterization techniques

A summary of experimental procedure and characterization techniques is shown in Figure 3.5.

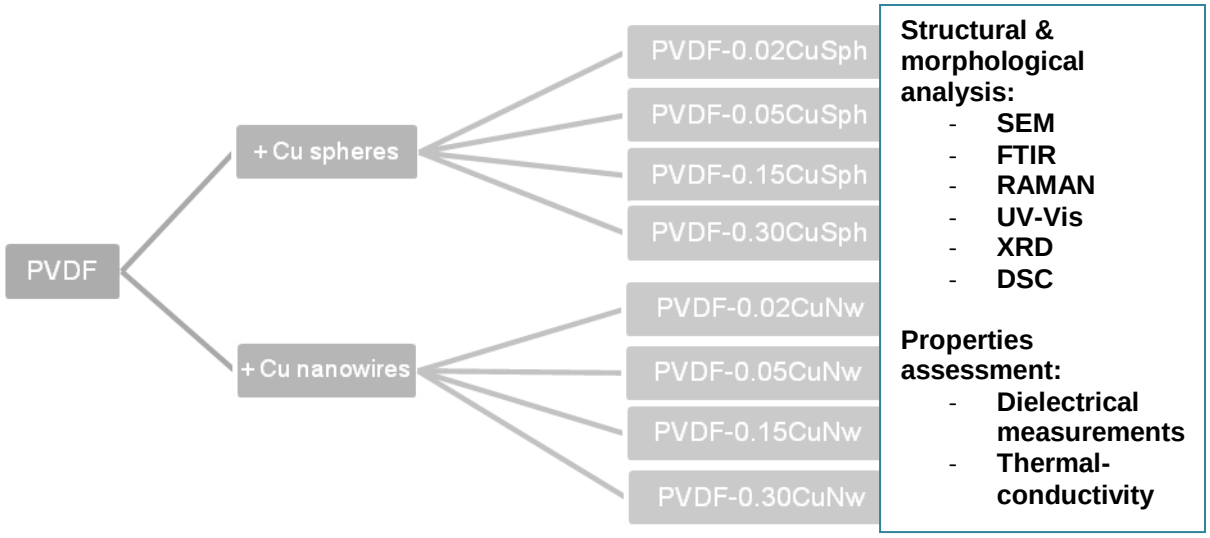

Figure 3.5 Scheme of experimental procedures and analyzed samples.

Table 3.3 lists the experimental methods used for sample investigation. The equipment and recording conditions are described.

Table 3.3 List of experimental methods used under current investigation.

Experimental method	Equipment	Recording conditions	Sample preparation	Notes
SEM	Hitachi SU-70 FEG-SEM	Voltage: 30 kV Magnification: 400, 500, 1000, 2000.	The films were coated with a conductive carbon layer.	Spherulites distribution was calculated by ImageJ.
FTIR	FTIR Mattson 7000 with ATR (Specac)	Recording range: 1700-300 cm^{-1} Resolution: 4 cm^{-1}	Both as prepared and pressed film	
Raman	Bruker RFS/ 100S	Power: 200 mW Resolution: 2 cm^{-1} Recording range: 3100 - 50 cm^{-1} Scans: 500	As prepared film.	Layers of film were imposed in the sample holder to increase sensitivity.
UV-Vis	Jasco V-560	Recording range: 850 - 220 nm Resolution: 0.5 nm. $BaSO_4$ was used as baseline.	As prepared film	
XRD	Rigaku Geigerflex	Continous measurement from 10^o to 80^o 2θ. Goniometer speed: 1^o 2θ/min.	As prepared film	
DSC	DSC-50 Shimadzu	Cell: aluminium seal Atmosphere: nitrogen Flow rate: 20 mL/min Temperature rate: 10 deg/min Temperature range: 25-230 ^oC.	Both as prepared and pressed film	Measurements performed in duplicate.
Dielectrical measurements	Impedance analyzer Hewlett-Packard 4284 A	Frequency range: 100 Hz-1MHz	Gold electrodes of 1.5 mm were vacuum deposited on pressed films.	Measurements performed in triplicate.
Thermal conductivity	TCi Mathis Model #: X-89	Contact agent: water. Gloves were used to minimize heat transfer from the hands.	The pressed film	7 measurements were taken for each sample.

4. Results and discussion

This chapter presents the results obtained in this work, concerning the preparation and characterization of PVDF/Cu nanospheres and PVDF/Cu nanowires. The microstructural and morphological results are first presented for each system and after related with the dielectric and thermal conductivity response. The relations between content and dimensionality of metallic nanoparticles with dielectric and thermal properties are established.

4. 1 Copper nanospheres and nanowires characterization

The morphology of synthesized copper nanoparticles was investigated by SEM. SEM micrographs revealed nanospheres with the diameter of 206±94 nm (Figure 4.1).

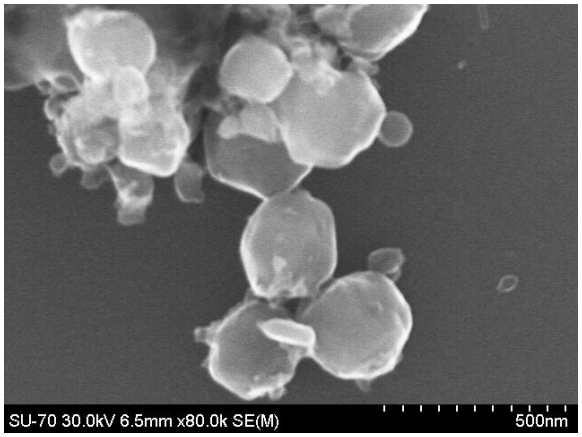

Figure 4.1 SEM micrograph of Cu nanospheres (offered with courtesy by Bruna Rosa).

UV-Vis of synthesized nanoparticles is displayed in Figure 4.2.

Spectral broadening and red shift of LSPR (local surface plasmon resonance) for Cu nanospheres is an evidence of particles oxidation[31].

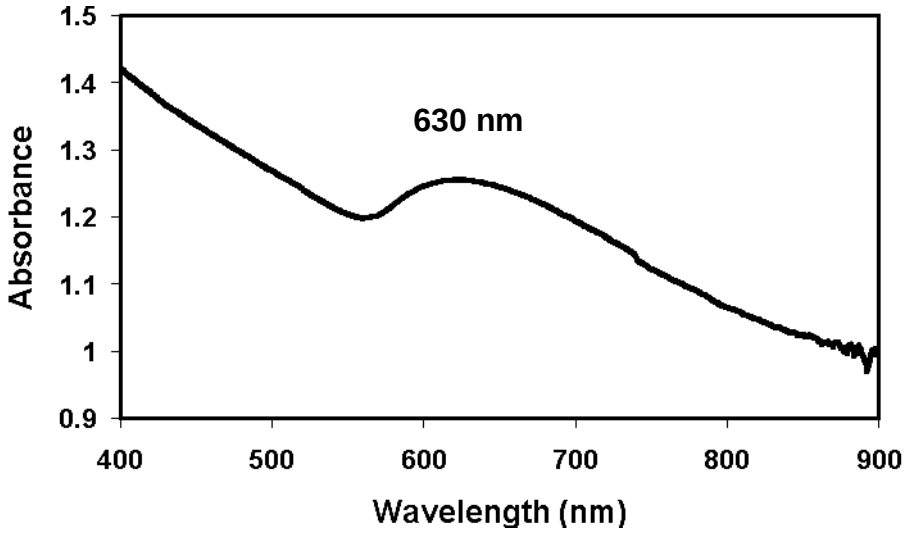

Figure 4.2 UV-Vis spectra of Cu nanospheres (offered with courtesy by Bruna Rosa).

Copper nanowires were investigated with X-ray diffraction (XRD) and UV-Vis. Morphological investigations were carried out with scanning electron microscopy.

Figure 4.3 shows SEM micrographs of Cu nanowires at different magnifications.

Based on SEM micrographs, the nanowires measure 317 ± 66 nm in diameter,10 ± 4 μm in length; with aspect ratio of 32 ± 12.

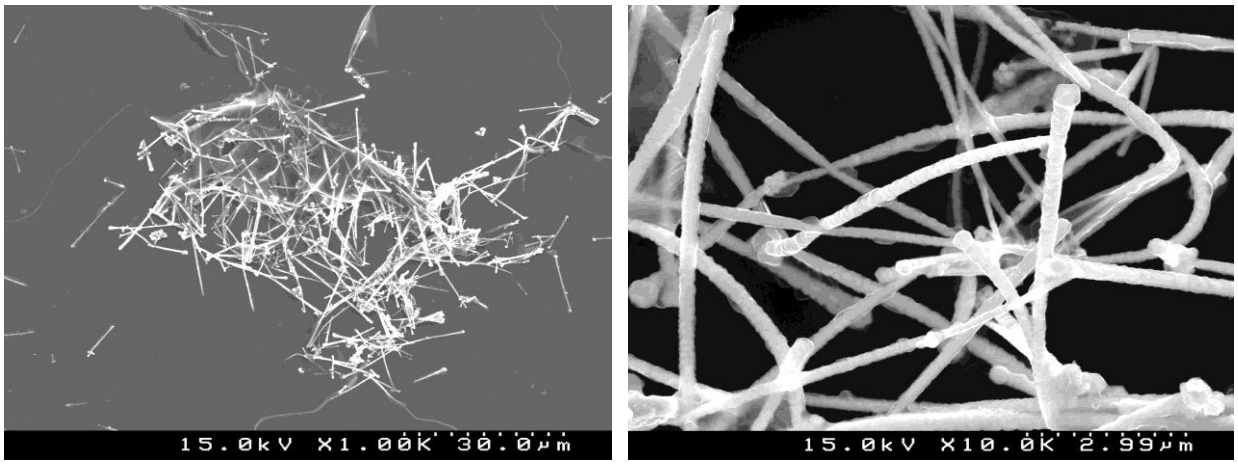

Figure 4.3 SEM micrographs of Cu nanowires (offered with courtesy by Ricardo João Borges Pinto).

Figure 4.4 displays UV-Vis spectra recorded for Cu nanowires. As expected for anisotropic Cu nanoparticles, the LSPR suffers a red-shift from expected value of 570-590 nm (as it is for spherical particles) to 604 nm. The LSPR peak is sharp, indicating that Cu nanowires are resistant to oxidation compared to Cu nanospheres (Fig. 4.4).

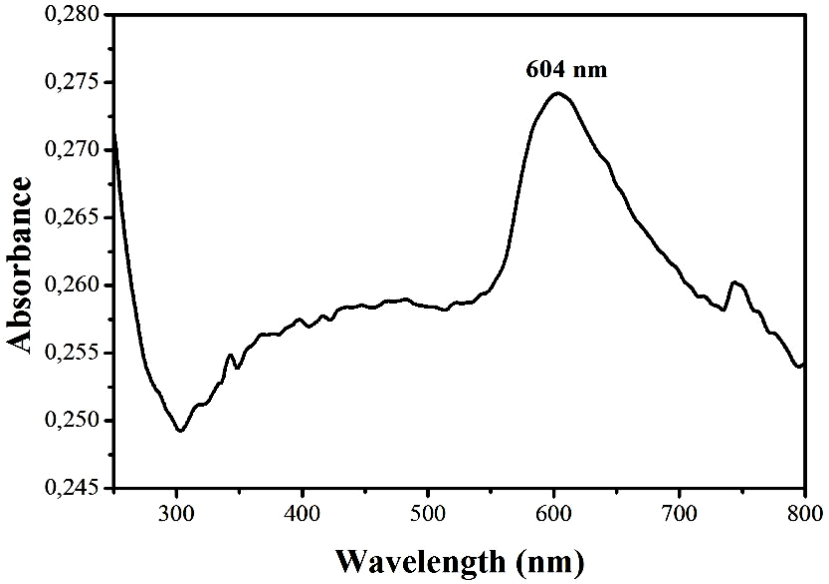

Figure 4.4 UV-Vis spectra of Cu nanowires (offered with courtesy by Ricardo João Borges Pinto).

XRD pattern of synthesized Cu nanowires (Fig. 4.5) displays three peaks at $2\theta = 43^{o}$, 50^{o}, 74^{o} which can be indexed to face-centered cubic copper[43]. No characteristic peaks of oxides impurities are detected.

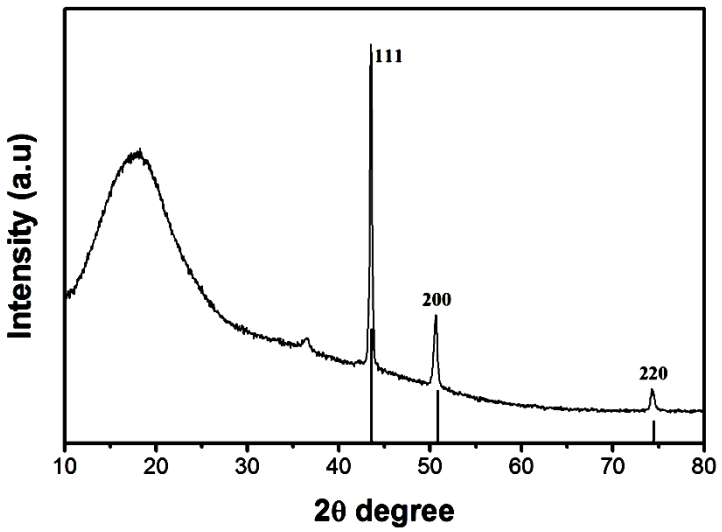

Figure 4.5 X-ray diffraction pattern of Cu nanowires (offered with courtesy by Ricardo João Borges Pinto).

4.2 Microstructural and morphological analysis

It is well known that the microstructure and the properties of a material are strongly interrelated. The structure, microstructure and morphology of PVDF/Cu composites were assessed by different methods. SEM was used to elucidate the microstructure of PVDF and PVDF/Cu composites. The elimination of porosity was also monitored with SEM. FTIR and Raman Spectroscopy was used for the determination of the polymer matrix phase. UV-Vis ad XRD offered valuable information concerning the Cu nanoparticles imbedded in the PVDF matrix. The influence of Cu addition on thermal properties of the polymer matrix was studied by DSC.

Pressed and unpressed samples of PVDF/Cu films were investigated by SEM for microstructure characterization, elemental mapping, as well as spherulites size distribution. Spherulites size distribution was calculated using ImageJ.

After film pressing, the porosity is almost entirely eliminated. The density of the pressed samples (Table 4.1) corresponds to the PVDF density listed in technical data sheet (1.75-1.80 g/cm^3)[44].

Table 4.1 Density and thickness of pressed and unpressed PVDF/Cu film samples.

Sample	Thickness* (μm)	Density (g/cm^3)	
		unpressed	pressed
PVDF	361±12	1.61	1.74
PVDF-0.02CuSph	363±29	1.67	1.78
PVDF-0.05CuSph	259±5	1.73	1.76
PVDF-0.15CuSph	270±4	1.62	1.80
PVDF-0.30CuSph	309±9	1.64	1.79
PVDF-0.02CuNw	348±3	1.61	1.76
PVDF-0.05CuNw	241±28	1.66	1.77
PVDF-0.15CuNw	220±57	1.65	1.77
PVDF-0.30CuNw	242±54	1.62	1.78

* the value of thickness indicated corresponds to pressed films

SEM analysis account as another evidence that porosity has been eliminated. Figure 4.6 illustrates SEM micrographs of PVDF-0.02CuNw film before and after pressing. The porosity has clearly disappeared.

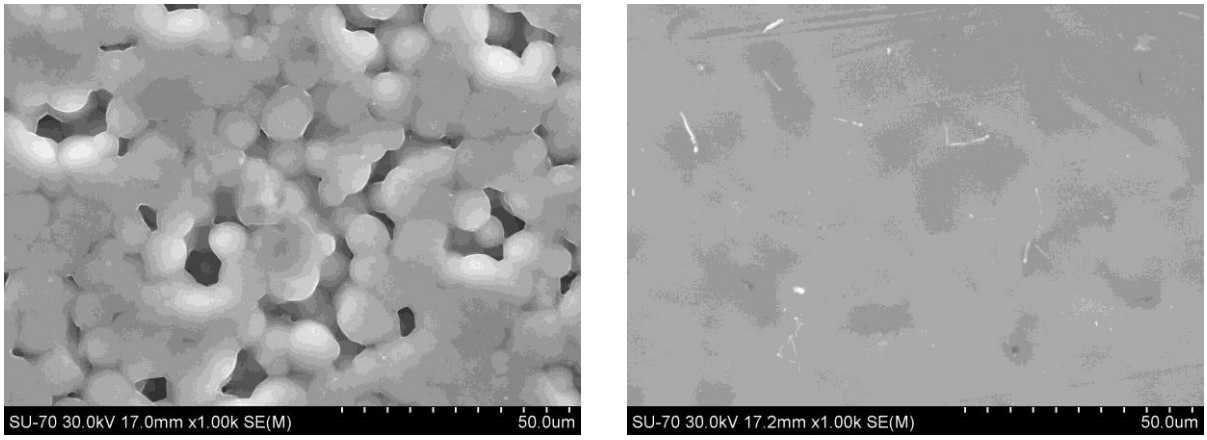

Figure 4.6 PVDF-0.02CuNw film before (left) and after pressing (right).

Many semicrystalline polymers that are crystallized from a melt form spherulites. The spherulites consist of aggregates of chain-folded crystalline lamellae that radiate from the center outward. Spherulites are considered to be the analogue of grains in polycrystalline metals and ceramics[45]. Concerning PVDF R. Gregorio and D. S. Borges[24] stated that β-phase shows spherical structure in SEM micrographs while α-phase displays radial lamellae.

SEM micrographs (Figs. 4.7, 4.8, and 4.10) show that PVDF films prepared in this work, regardless of the Cu content or dimensionality, crystallized in spherulitic structure.

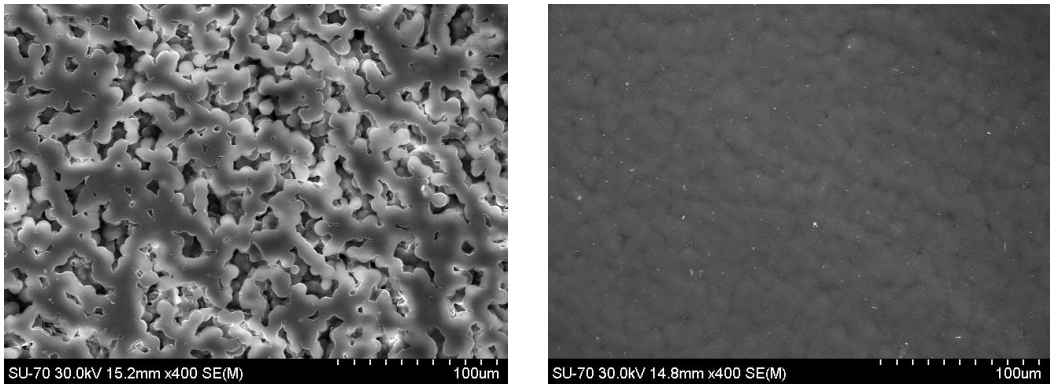

Figure 4.7 SEM micropraphs of pressed (right) and unpressed (left) films of PVDF.

Figure 4.8 presents the microstructures of unpressed PVDF/Cu spheres nanocomposites. For PVDF-0.02CuSph unpressed, the microstructure does not display porosity. The sample density of 1.67 g/cm^3 (Table 4.1) indicates the unpressed sample also contains porosity like other unpressed samples, although not shown in SEM micrograph. There is no obvious distinction between the rest of the samples: PVDF-0.05CuSph, PVDF-0.15CuSph, PVDF-0.30CuSph, in which the spherulites appear to be of same size. This statement is confirmed by spherulites size distribution (Fig. 4.9). There was no computation made for PVDF-0.02CuSph since the spherulites could not be distinguished. Analyzing the figure, it can be seen the following trend: the sizes of spherulites get slightly smaller with spherical Cu nanoparticles content increase, the highest spherulite size frequency moves from 9 μm in PVDF case to 5 μm for PVDF-0.30CuSph.

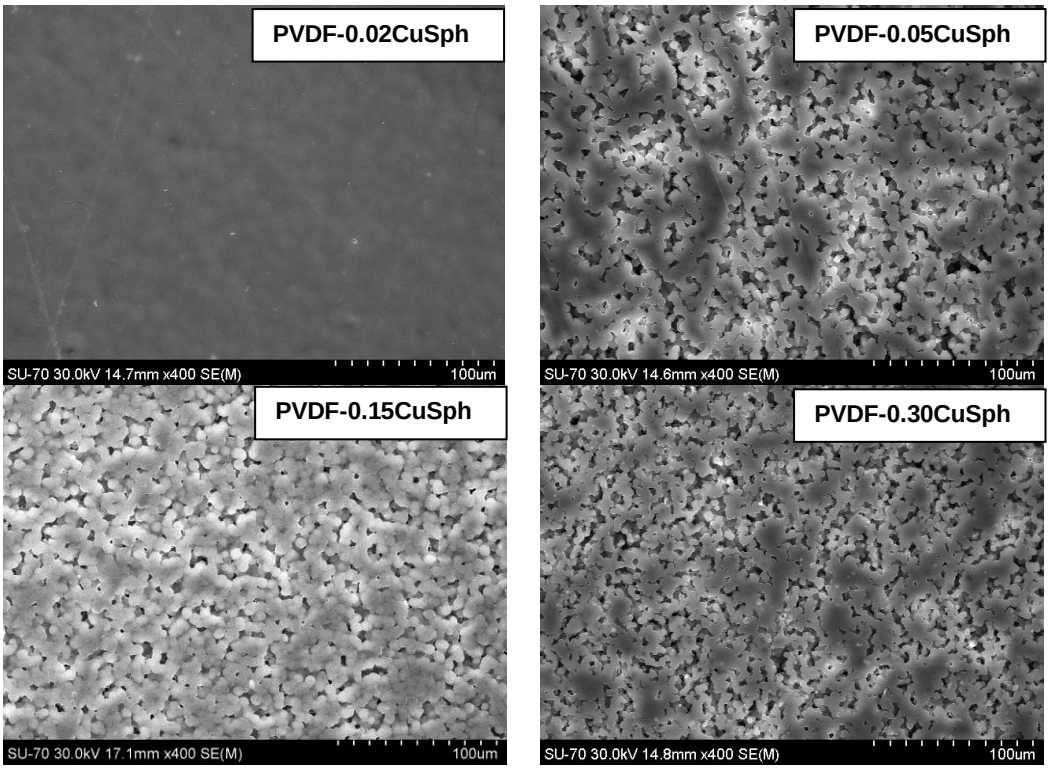

Figure 4.8 SEM micrographs of unpressed films of PVDF/Cu nanospheres.

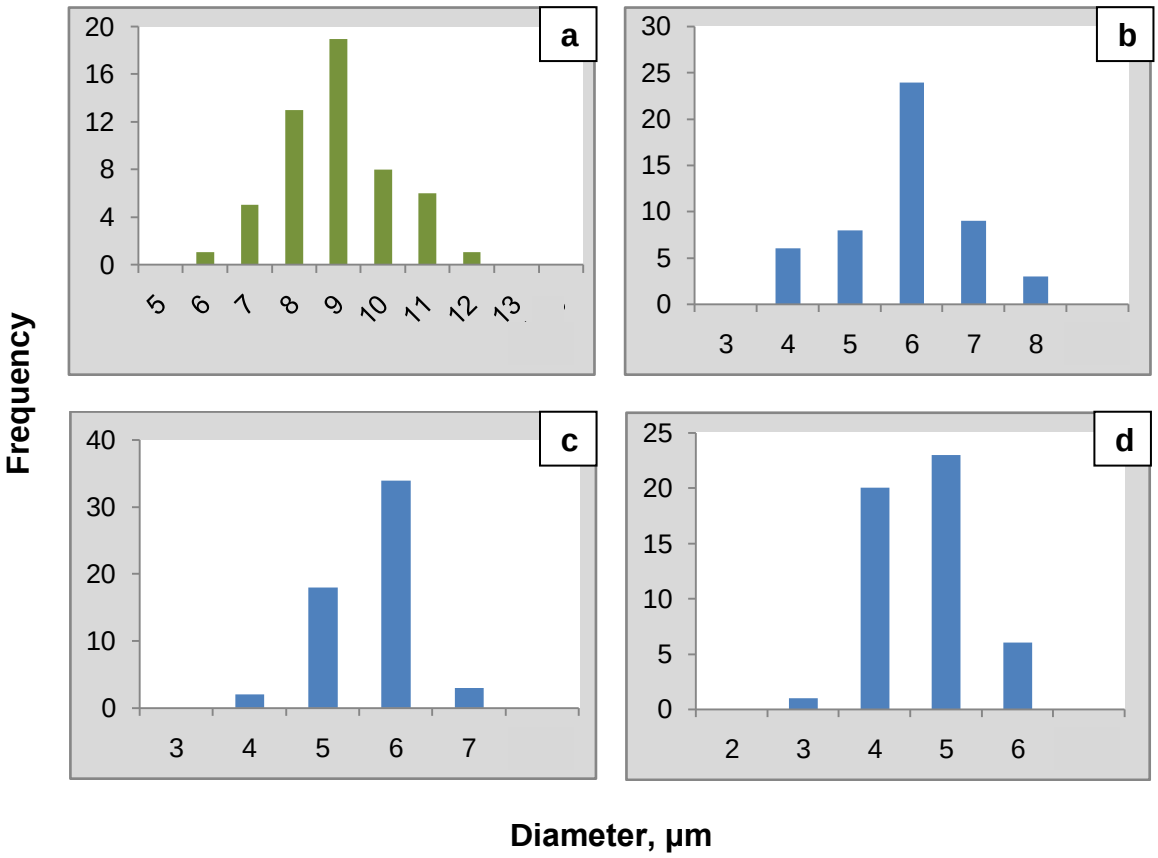

Figure 4.9 Spherulites distribution histogram for PVDF (green) and PVDF/Cu nanospheres (blue) samples a) PVDF b) PVDF-0.05CuSph c) PVDF-0.15CuSph d) PVDF-0.30CuSph.

Increasing the Cu nanospheres content results in a slight reduction of spherulite size in polymer matrix. Thus, Cu nanoparticles may be acting as nucleation sites to some degree and produce heterogeneous nucleation, promoting the formation of more spherulites but of smaller size.

PVDF/Cu nanowires nanocomposites present distinctive features when compared to PVDF/Cu spheres nanocomposites. Figure 4.10 illustrates the microstructures for nanocomposites containing Cu nanowires. Compared to spheres nanocomposites, the spherulites appear to be bigger in size, whereas there is no trend of spherulites size to increase in function of Cu nanowires content. There is an increase from 9 µm highest

frequency size to 20 μm for pure PVDF to PVDF-0.15CuNw (Fig. 4.11), followed by a depression of spherulite size in PVDF-0.30CuNw (9 μm).

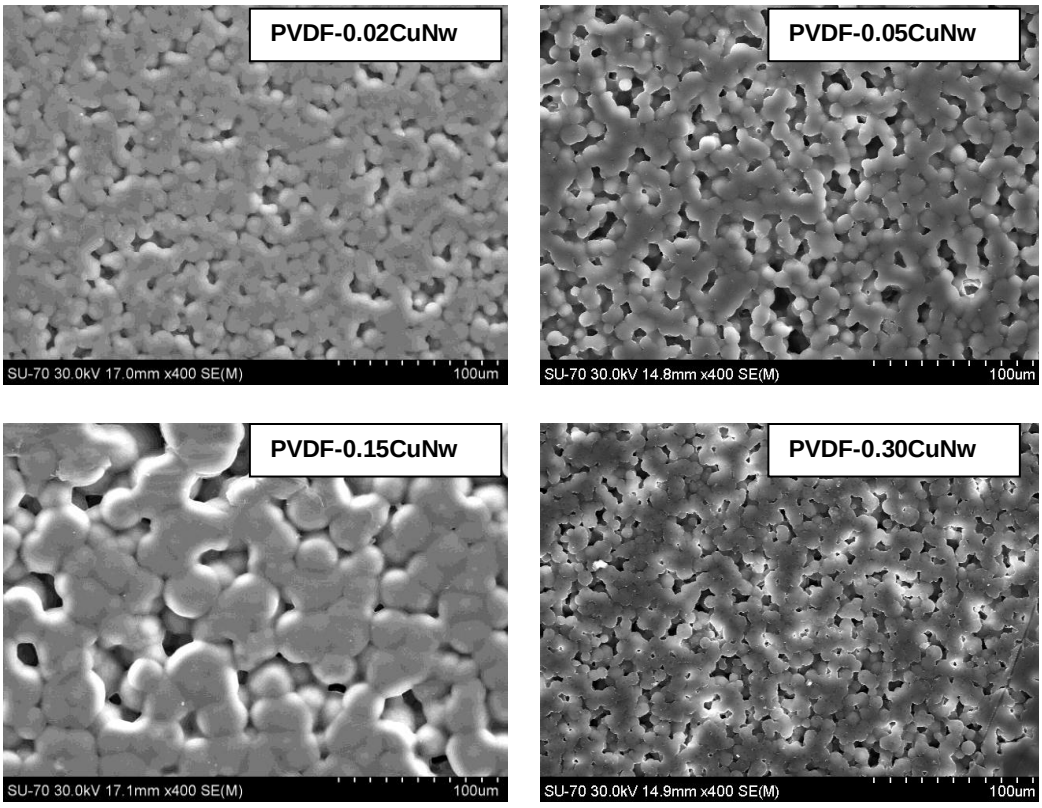

Figure 4.10 SEM micrographs of unpressed films of PVDF/Cu nanospheres.

Figure 4.11 illustrates the spherulites distribution histograms for PVDF/Cu nanowires composites. Generally, larger crystallite sizes are produced when Cu nanowires content is increased. Hence, fewer nucleation sites are formed and larger crystallites are generated. Probably, the anisotropy of Cu nanowires acts as a negative factor in nucleation sites formation. An exception is observed for PVDF-0.30CuNw (Fig.4.11 d) where the spherulites size decreases comparable to pure PVDF (Fig. 4.9 a).

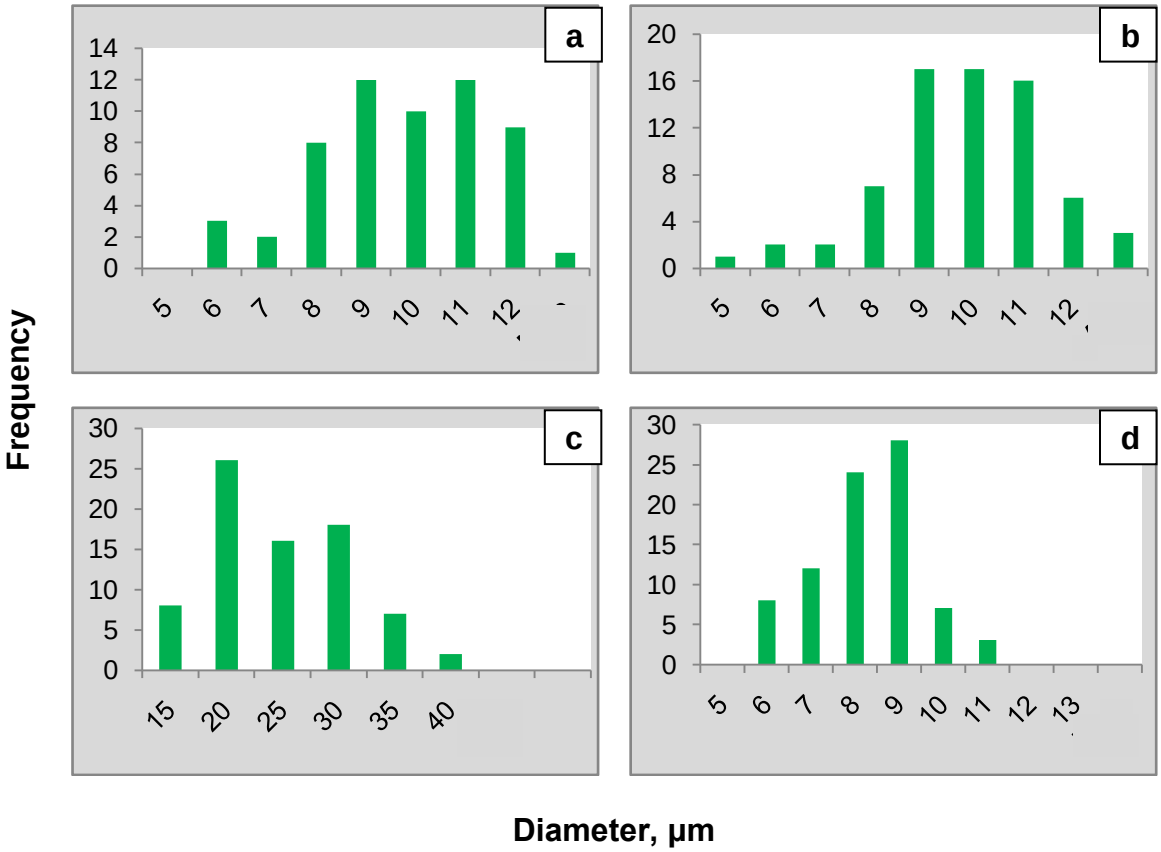

Figure 4.11 Spherulites distribution histogram for PVDF/Cu nanowires (green) samples a) PVDF-0.02CuNw b) PVDF-0.05CuNw c) PVDF-0.15CuNw d) PVDF-0.30CuNw.

It can be seen in Figure 4.12 that Cu spheres and Cu nanowires are randomly distributed in the PVDF matrix with agglomerations. Spherical nanoparticles as shown in Figure 4.12, due to higher specific surface tend to agglomerate more in comparison to nanowires. Cu nanowires occur mostly individually in PVDF matrix without noticeable preferred orientation.

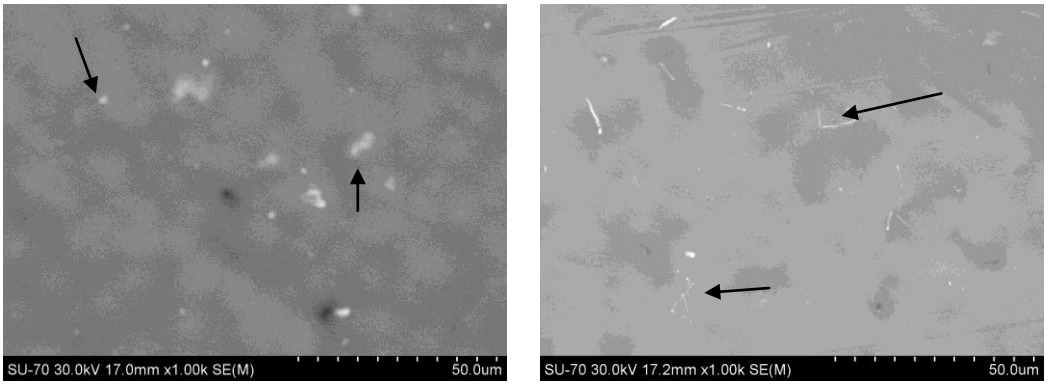

Figure 4.12 SEM micrographs of PVDF-0.02CuSph (left) and PVDF-0.02CuNw (right). Both samples are pressed. Arrows indicate Cu nanoparticles.

FTIR is a powerful tool when applied to phase characterization of PVDF. FTIR technique gives the possibility to distinguish qualitatively between α, γ, and β phases. Moreover, when β phase is present in large amounts the quantitative phase amount can be easily deducted from absorption peaks[8].

In spite of significant effort directed to interpret the IR spectrum of PVDF, the literature data remains contradictory. Table 4.2 presents a summary with vibrational mode wavenumbers of PVDF adapted after Y. Bormashenko et al[23].

Table 4.2 Vibrational mode wavenumbers (cm^{-1}) of PVDF (the peaks of interest are marked with black bold for γ-phase, blue bold for β-phase, and green bold for both β- and γ-phase).

Band (cm^{-1})	Phase	Group or vibrational mode
483	γ	
489	α	
511	**β or γ**	CF_2 bending
530	α	CF_2 bending
615	α	CF_2 bending and skeletal bending
678		Polymer chain defects due to head-to-head, tail-to-tail linkages
766	α	CF_2 bending
778	γ	CH_2 rocking
795	α	CH_2 rocking
812	**γ**	CH_2 out-of-plane wag
834	**γ**	
840	**β or γ**	CH_2 rocking
855	α	CH out-of-plane deformation
976	α	CH out-of-plane deformation
1234	**γ**	CH out-of-plane deformation
1279	**β**	CH out-of-plane deformation

Further according to Gregorio et al.[24], 408 cm^{-1} peak corresponds to α-phase, 444 cm^{-1} to γ-phase, and 431 cm^{-1} to β-phase.

Bormashenko et al[23] gives special attention to 600 cm^{-1} peak. The author considers reasonable to relate it to β-phase, since the intensity of the peak increases with β-phase volume fraction in PVDF membrane.

The FTIR spectra recorded for various PVDF phases are given in Figure 4.13.

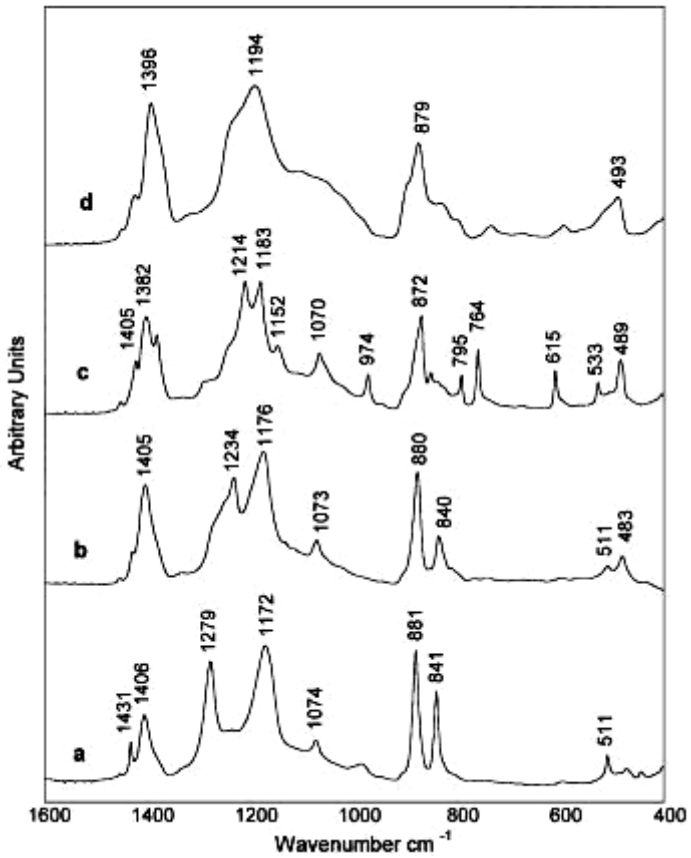

Figure 4.13 IR spectra of thin PVDF samples for a) α-phase (solution casted) b) γ-phase (solution casted) c) β-phase (solution casted) d) melt[25].

The absorption bands of PVDF/Cu samples can be assigned to certain polymer phase indicating the predominant phase of polymeric composites.

There is still a huge debate about β- and γ-phase synthesis through solution casting method. Some authors argue that exclusively β-phase is formed when PVDF is casted at temperatures lower than 70 ^{o}C regardless the used solvent [13,24]. Tashiro et al [8] suggest that low crystallization rates favor the formation of trans conformations whereas high rates the gauche conformations. On the other hand, crystallization rate depends on evaporation rate of the solvent, which is closely related to the evaporation temperature, solution concentration, relative humidity[24]. M. Benz and W. B. Euler obtained PVDF films with predominantly γ-phase after casting from a solvent composed of 90 % acetone and 10 % DMF and temperature

bellow 80°C[37]. Solution-crystallized PVDF in N,N - dimethylacetamide (DMAc) at low temperatures is reported to form mainly β- or γ-phase[38]. Higher humidity supposedly promotes a higher fraction of γ-phase[37].

In addition researchers are still disputing around β- and γ- phase identification using vibrational spectroscopy[23]. Because of almost similar structures within these two phases, most of the vibrational modes are characteristic for both of them, making the identification of specific features very difficult. In this work, the spectra assessment was made according to Table 4.2.

Figure 4.14 illustrates FTIR spectra for PVDF and PVDF/Cu nanospheres. Clearly, according to Table 4.2, the polymer matrix contains γ-phase (1234, 834, 812, 431 cm^{-1}) in a large extent with small content of α-phase (612, 408 cm^{-1}). The characteristic peaks for β-phase (1275, 445 cm^{-1}) appear weak and undecipherable.Qualitatively, the spectra appear to be the same regardless of Cu spheres content in polymeric matrix: no new modes appear or are being surpressed.

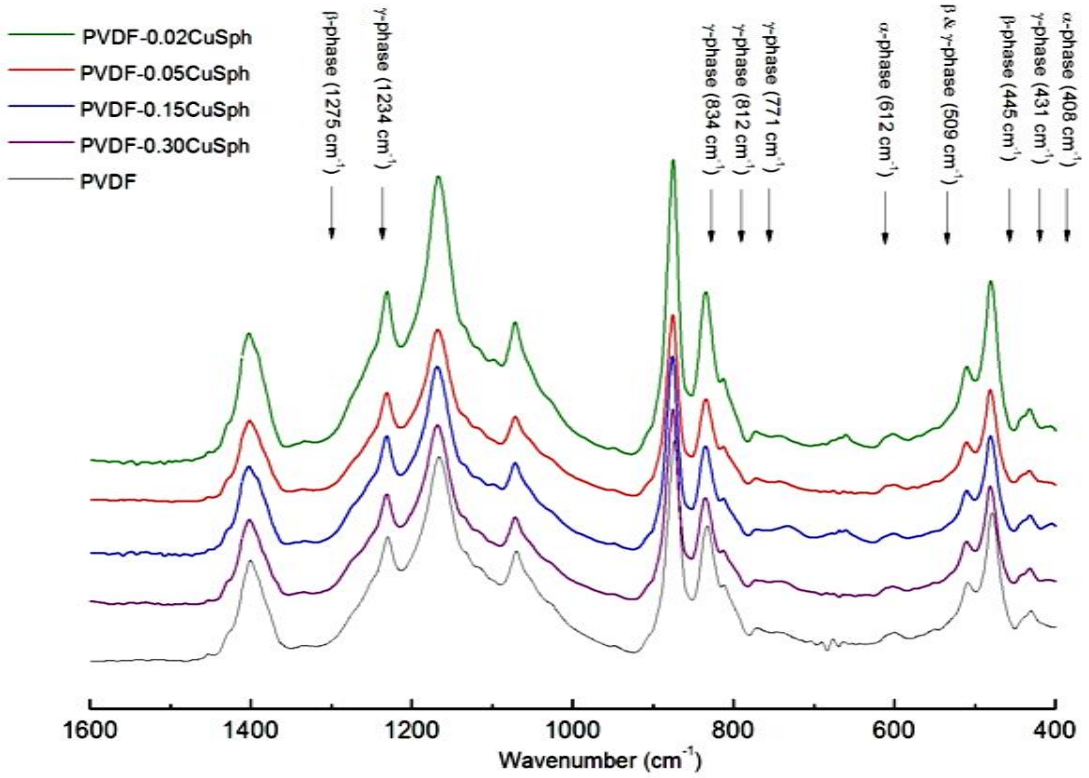

Figure 4.14 FTIR spectra of PVDF/Cu nanospheres composites with different Cu content.

Figure 4.15 illustrates FTIR spectra for PVDF and PVDF/Cu nanowires. First to notice, there are no qualitative differences within the spectra of composites with different Cu nanowires content in polymeric matrix. As in the case of PVDF/Cu nanospheres, the polymeric matrix crystallized mostly in γ-phase with scarce inclusions of β- and α-phases. The specific vibration modes for β-phase appear as shoulders, also. Moreover, there are no differences in the FTIR spectra of PVDF, PVDF/Cu nanosheres, and PVDF/Cu nanowires: inclusion of nanoparticles with different content, dimensionality, and shape has no relevant effect in the phase in which the polymer crystallizes.

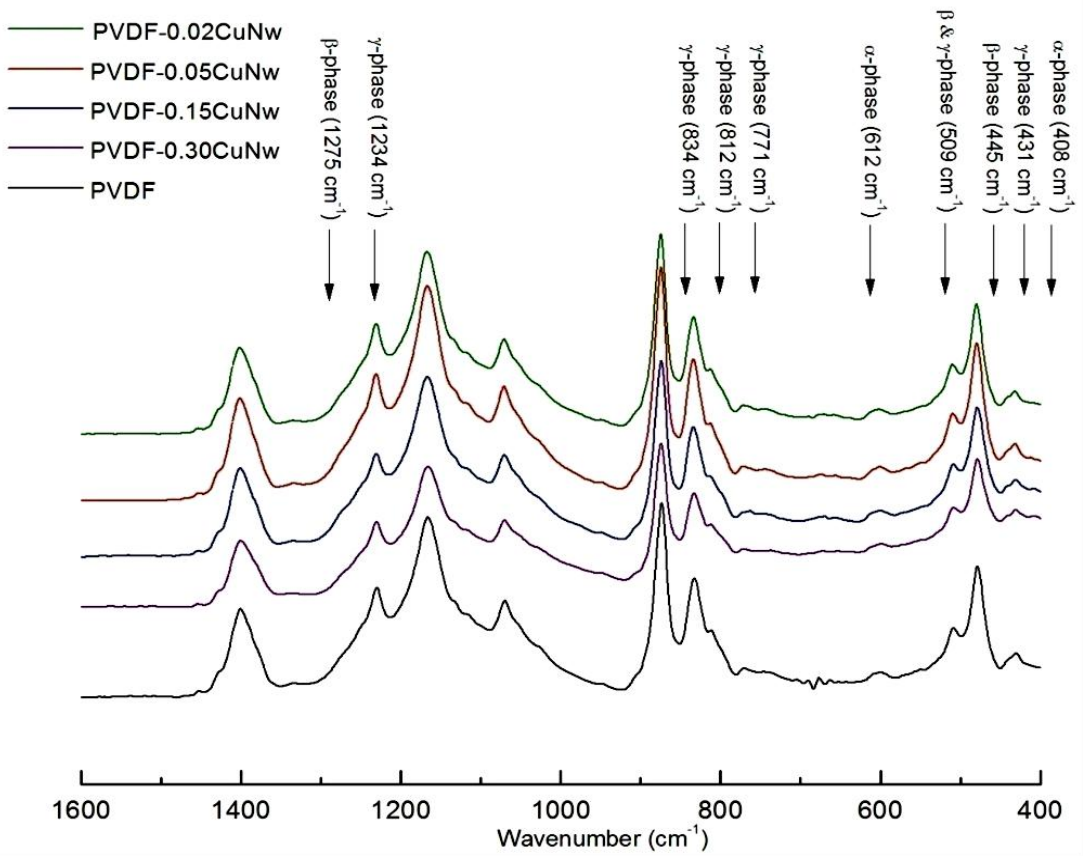

Figure 4.15 FTIR spectra of PVDF/Cu nanowires composites with different Cu content.

The pressed and unpressed samples do not exhibit differences in FTIR spectra (Fig. 4.16). The sample pressing did not produce any change concerning the polymer conformation. FTIR spectrum of the pressed sample displays same vibrational modes as the unpressed one.

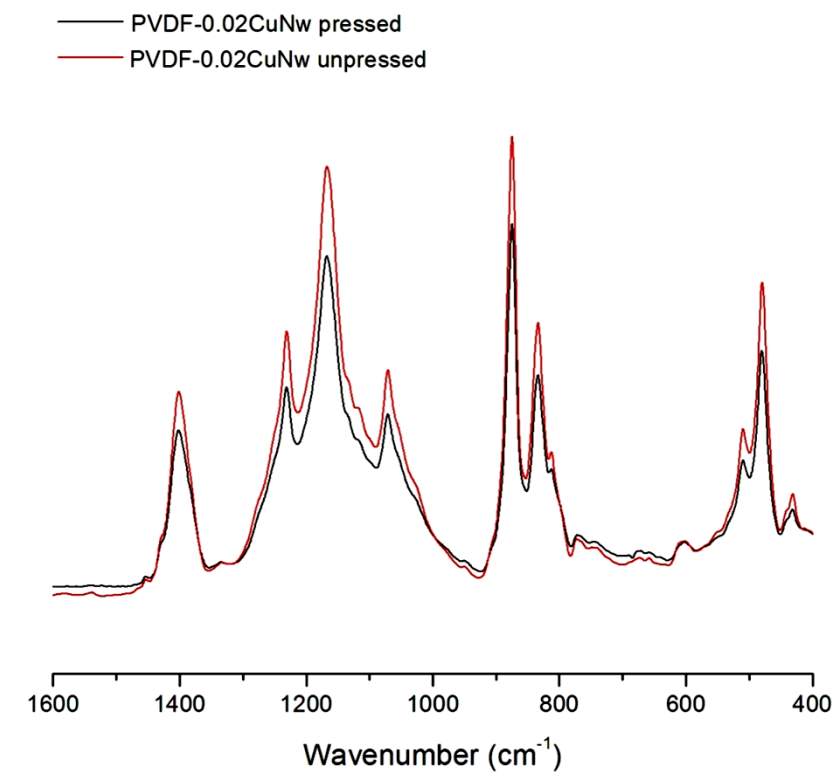

Figure 4.16 FTIR spectrum of pressed (black) and unpressed (red) PVDF-0.02CuNw films.

Raman spectroscopy is employed as a complementary tool for FTIR to investigate and distinguish within the phases adopted by PVDF and its composites.

Table 4.3 collects the characteristic Raman shifts for α, β, and γ-phases of PVDF as ascribed by various authors.

Table 4.3 Characteristic Raman shifts for different conformations of PVDF.

	α-phase	β-phase	γ-phase	Reference
Raman shift, cm^{-1}	612, 795	840	not reported	27
	795	839 (very strong only for β)	839, 811 (characteristic only for γ)	25
	795, 875	not reported	841, 810	28

Figure 4.17 shows Raman spectra as cast from different solvents[25]. The Raman spectrum for PVDF casted from DMF (Fig. 4.17 a) contains a band at 839 cm^{-1} which according to the author is common to both β and γ phase but is strong only for form β.

The appearance of the band at 811 cm^{-1} is assigned to γ-phase and it indicates an important amount of T_3G sequences[25]. The band characteristic for α-phase appears only as a shoulder: TG sequences have a very minor contribution to the polymeric structure. Based on the Raman spectra above it is concluded the overall polymeric structure consists of trans zig-zag conformations typical for β-phase with an important content of γ-phase.

In case of PVDF casted from NMP the spectrum remains basically the same as casted from DMF (Fig. 4.17 b).

For PVDF casted from TEP, the specific Raman shift for γ-phase almost disappears meanwhile the band assigned to α-phase increases, indicating the presence of all trans chains with TG crystalline domains (Fig. 4.17 c).

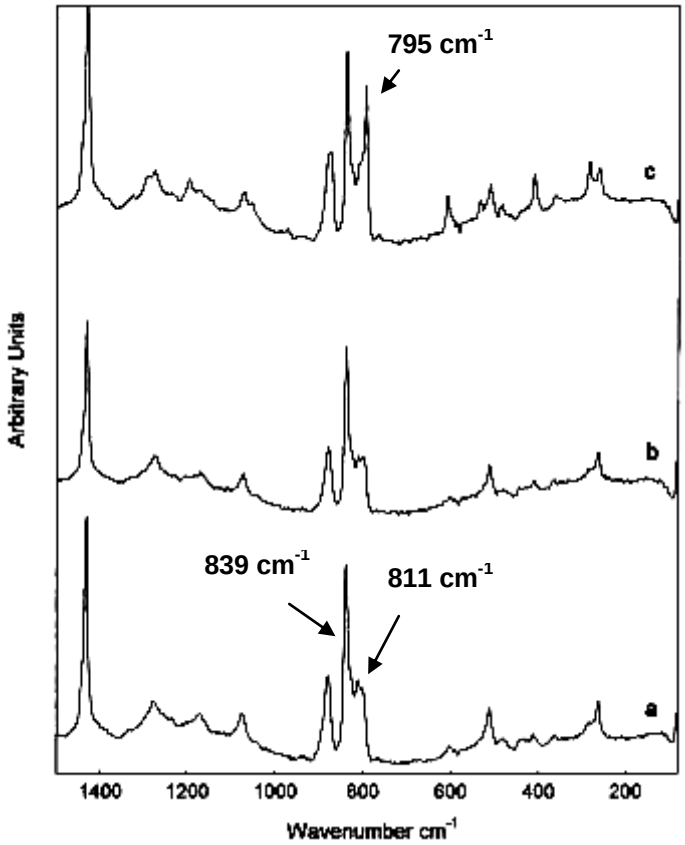

Figure 4.17 Raman spectra of PVDF membranes cast from: a) DMF b) NMP (N-Methyl-2-pyrrolidone) c) TEP (triethyl-phosphate)[25].

Figure 4.18 shows the Raman spectra of PVDF/Cu nanospheres. As in the case of FTIR spectra, there are no qualitative differences within spectra. The band at 839 cm^{-1} characteristic for both β- and γ-phases (Table 4.3) can be recognized distinctly. This band is strong only for β-phase[25]. In our case, the band at 811 cm^{-1} characteristic for γ-phase is stronger than one at 831 cm^{-1}, meaning the polymer matrix comprises an important amount of T_3G conformation typical for γ-phase with a content of α-phase (795, 875 cm^{-1}) and traces of β-phase. Regardless of Cu spheres content, the bands appear to be the same. Raman spectroscopy confirms the analysis done with FTIR spectroscopy: γ-phase bands appear predominantly in the spectra of the nanocomposites.

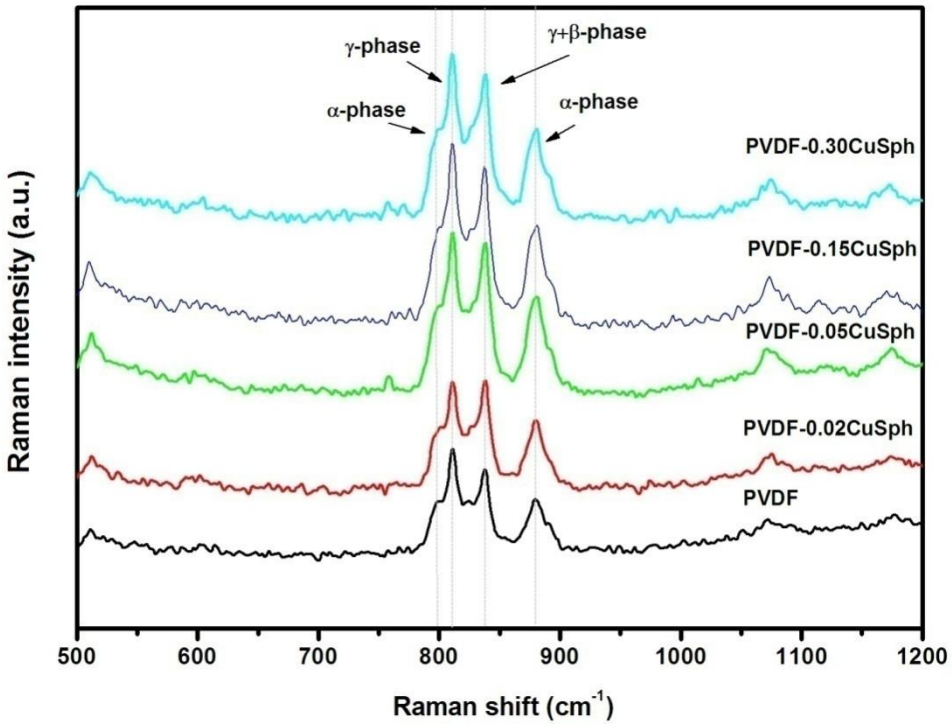

Figure 4.18 Raman spectra of PVDF/Cu nanospheres composites with different Cu content.

Figure 4.19 shows Raman spectra for PVDF/Cu nanowires composites. When imbedded with Cu nanowires nanoparticles, the films turned to a brownish color; the intensity of color increased with nanoparticles concentration, so Raman spectra could not be recorded for PVDF-0.30CuNw.

As in the case of PVDF/Cu nanospheres, Raman spectroscopy confirmed the presence of γ-phase in a large extent, and a small amount of α-phase as traces of β-phase for PVDF/Cu nanowires. Furthermore, qualitatively Raman spectra are similar for both PVDF/Cu nanospheres and PVDF/Cu nanowires.

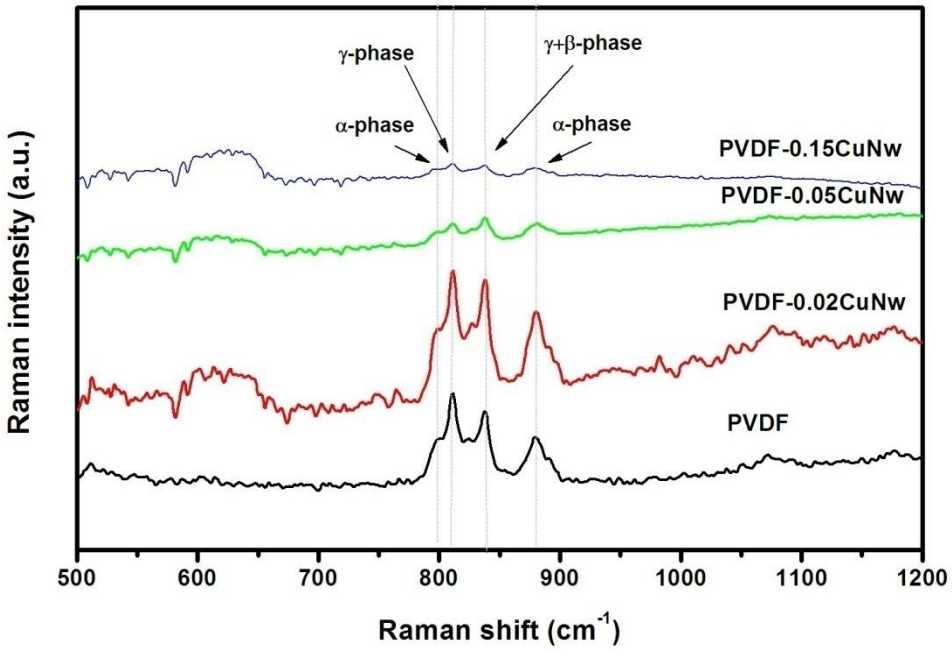

Figure 4.19 Raman spectra of PVDF/Cu nanowires composites with different Cu content.

Both UV-Vis and XRD analysis were performed to confirm the presence of Cu nanoparticles in the polymeric matrix film as to assess qualitatively the films composition.

During the preparation process as when films are exposed to air, Cu nanoparticles are expected to oxidize. So, pure Cu and Cu oxides are expected to be found in film samples.

A very useful diagnostic to study nanoparticles is UV-Vis spectroscopy. Because of their small size, electrons in metal nanoparticles become confined. These confined electrons are excited to oscillate within the cluster giving so called local surface plasmon resonances (LSPR).

The formation of the local surface plasmon resonances can be seen as following (Fig. 4.20): when an electromagnetic field is applied on the nanoparticle, this field induces a dipole[30]. There is a restoring force which tries to compensate the formed dipole. Therefore,

the conduction electrons of the nanoparticle oscillates with a unique resonance frequency to match the incoming electromagnetic radiation.

Metals like Pb, In, Hg, Sn, Cd give plasma frequencies in the UV part of the spectrum and the nanoparticles of these metals do not display strong color effect. Also, the nanoparticles of these metals being small, oxidize easily, and that makes their UV-Vis investigation difficult. UV-Vis spectra are mostly recorded on more noble and air-stable colloid of Ag, Au, Cu nanoparticles. Because of d-d transitions, the LSPR of these metals is pushed in the visible part of the spectra[30].

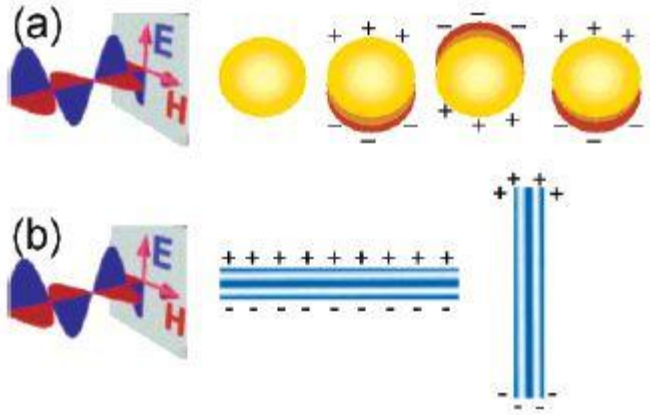

Figure 4.20 a) Interaction of the electromagnetic radiation with a metal nanosphere. The electromagnetic radiation induces a dipole moment in the nanoparticle which oscillates in same phase with the light of the electric field b) Transversal and longitudinal oscillation of electrons in a metal nanorod[30].

The frequency of LSPR depends on the nature of metal, size, shape, and presence of capping shell on the particle surface, dielectric properties of the surrounding medium[30]. This phenomenon is illustrated in detail in Figure 4.21 on the example of Au nanoparticles. The shape of the nanoparticle influences in a higher extent the frequency of LSPR than the nanoparticle size[30-32]. When the particle possesses an anisotropic shape, both transversal and longitudinal oscillations are possible (as displayed in Figure 4.21 b) depending on the orientation of the electric field relative to the particle[30].

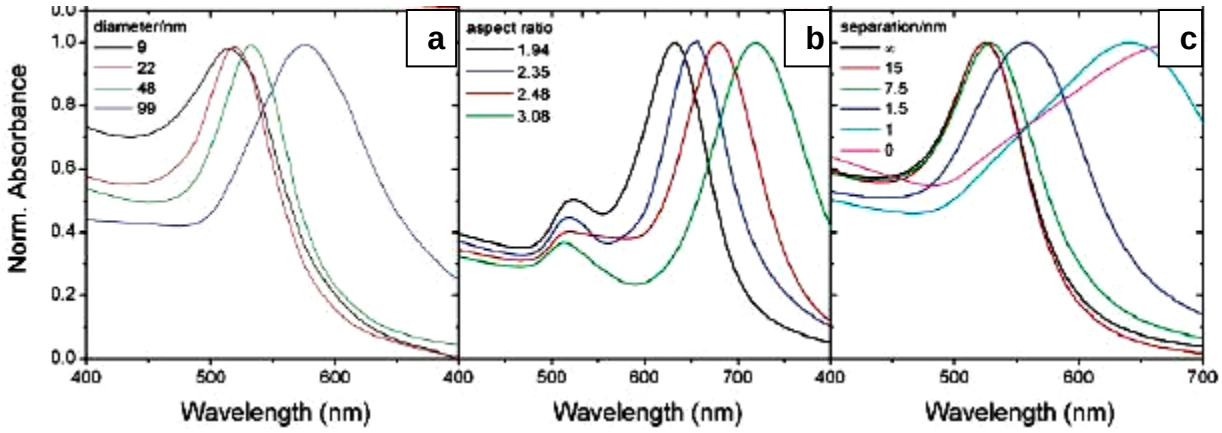

Figure 4.21 UV-Vis spectra for a) Au spheres with varying diameter b) Au nanorods with varying aspect ratio c) multilayer films of glass-coated Au spheres with varying interparticle distance[30].

Comparing to noble metals like Ag and Au, Cu has a dielectric function which is subjected to lower energy interband transitions (~2.15 eV) and also is prone to oxidation. The characteristic frequencies of isotropic Cu nanoparticles lie in the range of 565-590 cm^{-1}. With increase in anisotropy, the LSPR frequency is pushed in the red part of the UV-Vis spectrum[30,31]. The oxidation plays an important role in the observed LSPR spectra of Cu. It is reported a temporal change of LSPR of anisotropic Cu during oxidation followed by a gradual red-shift and spectral broadening[31]. According to Ref. 31, there is no LSPR peaks observed in case of Cu with size of few nanometers: Cu has a low stability against oxidation causing rapid conversion of Cu to Cu_2O. There is no LSPR peak observed from Cu_2O spectra.

By imbedding metal nanoparticles in a polymeric film, it is possible to synthesize materials with optical properties which lie between transparent films and metallic particle[32]. There are theoretical models which predict the LSPR frequency of the composite by calculating the average dielectric function of the medium taking into account both components: the nanoparticles and the matrix. Maxwell-Garnet theory[32] gives better results for small spheres distributed isotropically among the matrix, while Bruggerman theory[32] accounts better for other cases.

There is no literature data found for Cu nanoparticle polymer films for UV-Vis data. Ref. 32 describes Au nanoparticle thin films and states that dipole interaction of the particles promotes a red-shift and a broadening of the plasmon resonance. As it can be seen in Figure

4.21 c, the dipole interaction is stronger when the interparticle distance decrease, which is followed by red-shift and broadening of LSPR with decrease of separation within particles.

As expected, only samples with higher Cu content show LSPR band in UV-Vis spectra (Figs. 4.22, 4.23).

Analyzing the UV-Vis spectra for PVDF/Cu nanospheres (Fig. 4.22), only the samples PVDF-0.15CuSph and PVDF-0.30CuSph exhibits the peaks, at 588 and 612 nm, respectively. There is a red shift for PVDF-0.30CuSph which can be explained through the decrease of interparticle distance since the amount of Cu is high. When the interparticle distance is decreased, dipole interaction between the particles is higher promoting a red-shift and broadening of plasmon resonance[31].

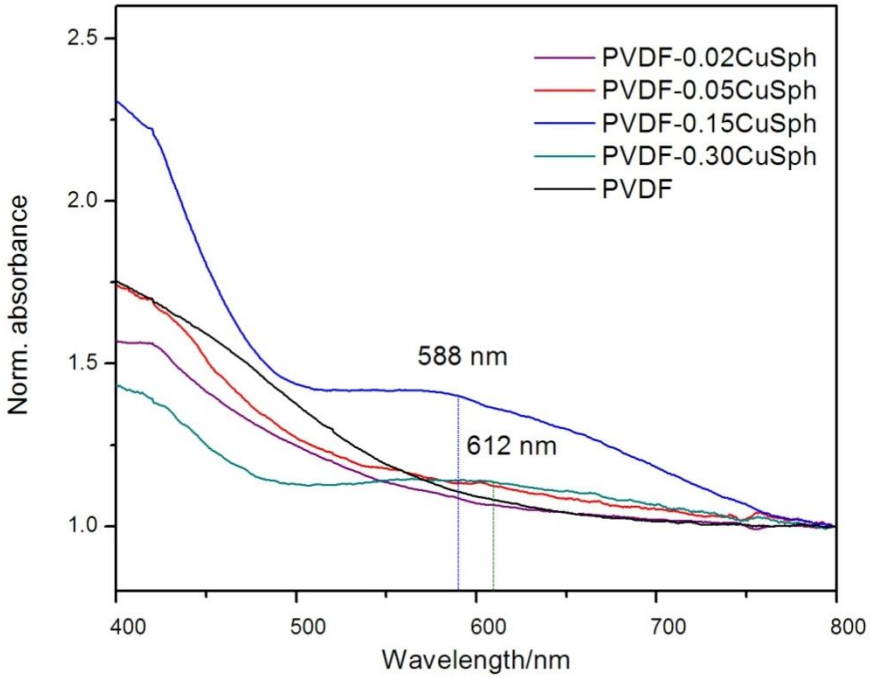

Figure 4.22 Normalized UV-visible spectra of PVDF/Cu nanospheres composites with different Cu content. All spectra were normalized to 1 at 800 nm for better comparison.

Figure 4.23 represents UV-Vis spectra for PVDF/Cu nanowires. The LSPR peak appears only in the case of PVDF-0.30CuNw, although the curve goes blunt for PVDF-0.15CuNw indicating the finger print of a peak.

Unexpectedly, the peak of PVDF-0.30CuNw suffers a blue shift, although it is argued that anisotropy should produce a red shift of LSPR peak[30,31]. This blue shift was noticed also in the work of D. Miranda *et al.* and might be due to two combined effects: refractive index of the polymer and scattering contribution related to the film thickness[5]. The blue-shift of the PVDF-0.30CuNw in respect to the PVDF-0.30CuSph occurred probably due to higher scattering observed in its spectrum.

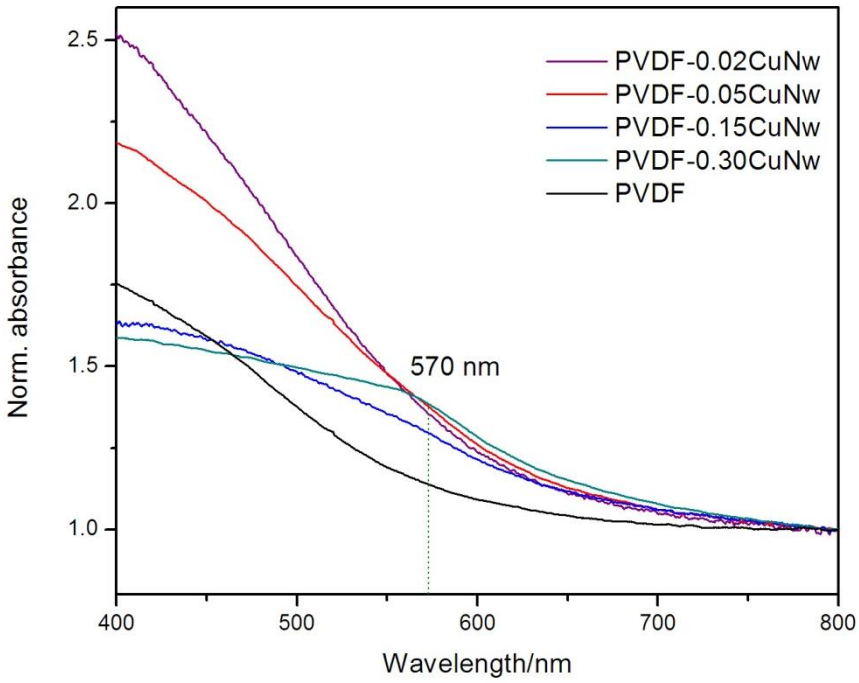

Figure 4.23 Normalized UV-visible spectra of PVDF/Cu nanowires composites with different Cu content. All spectra were normalized to 1 at 800 nm for better comparison.

To notice LSPR in case of films imbedded with nanospheres is broader than the one for nanowires composites. It is argued that Cu nanoparticles oxidation results in broadening of LSPR band[31], indicating the ease of oxidation for spherical Cu nanoparticles in relation to nanowires ones.

XRD was performed to identify the presence of copper and copper oxides in the polymeric matrix. It is not straightforward to distinguish PVDF phases through XRD analysis. Most of the peaks of different phases are situated close to each other, so there cannot be made an accurate assumption about the phases contained in the polymeric matrix without FTIR or

Raman spectroscopy. Table 4.4 summarizes the values of 2θ and respective d spacing for each phase.

Table 4.4 Values of 2θ and respective d spacing for each phase. The data is collected from literature.

Phase	2θ	d(Å)	Reference
α	18.20	4.87	34
	19.71	4.50	
	28.87	3.09	
	30.81	2.90	
	34.74	2.58	
	35.60	2.52	
	38.61	2.33	
	42.61	2.12	
β	20.26	4.38	35
α+γ	17.66	5.01	13
	18.30	4.84	
	20.04	4.42	
	26.56	3.35	

No peaks for Cu were found in the XRD patterns for PVDF/Cu nanospheres composites (Figure 4.24). Lack of Cu signal can be explained through very low nanoparticle content as the Cu spheres most probably oxidized when exposed to air. Signals for CuO and Cu_2O were also not found (for none of the composites).

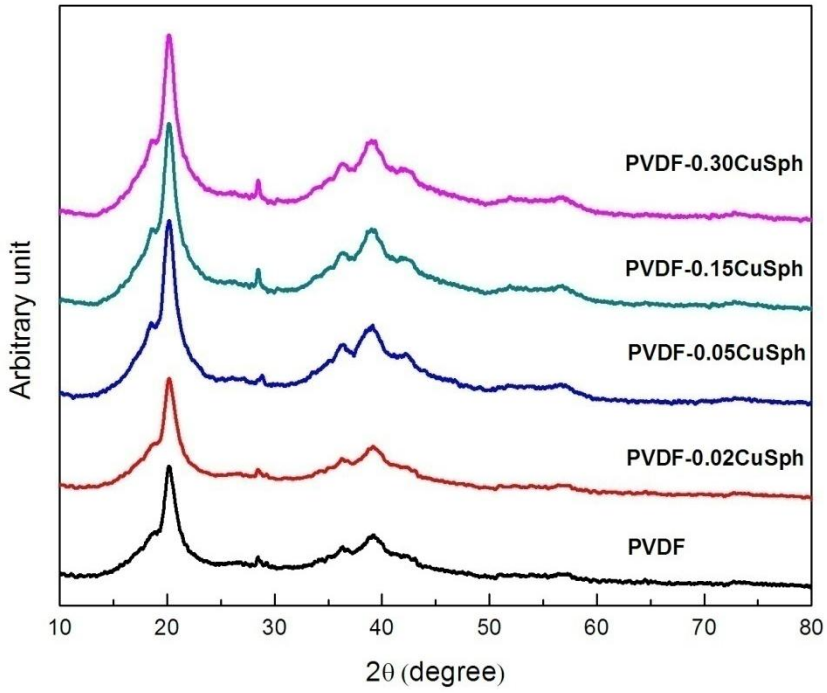

Figure 4.24 XRD patterns of PVDF/Cu nanospheres composites with different Cu content.

The signal for Cu was found only in case of PVDF-0.30CuNw, the sample with highest Cu nanowires content (Fig. 4.25). There were no peaks found for copper oxides.

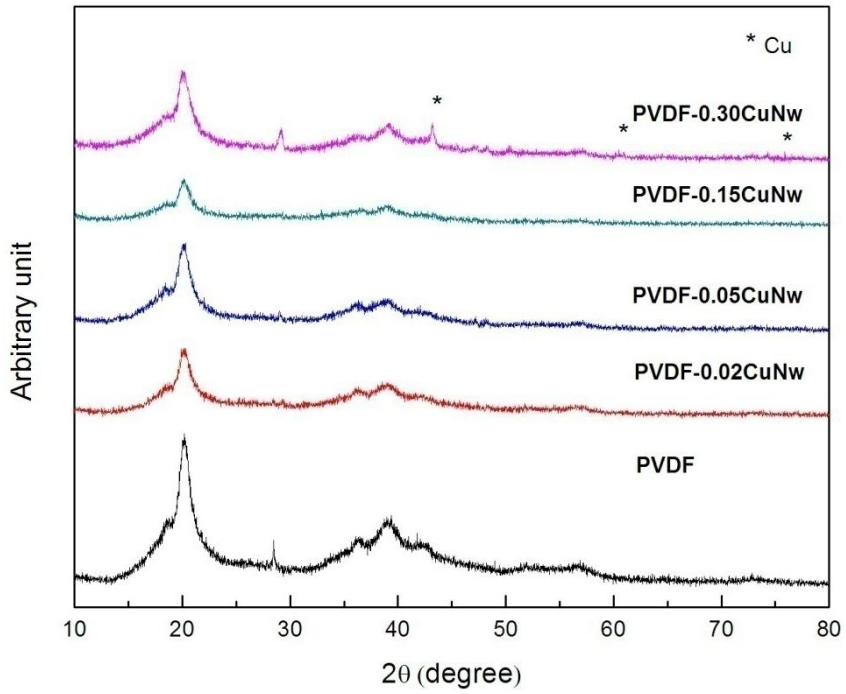

Figure 4.25 XRD patterns of PVDF/Cu nanowires composites with different Cu content.

Thermal behavior, melting temperature and degree of crystallinity of pure PVDF and PVDF/Cu nanowires were investigated with Differential Scanning Calorimetry (DSC).

DSC is an important method to collect thermal data like melting temperature(T_m) and heat of fusion (ΔH_f). Moreover, it allows computing the polymer matrix degree of crystallinity (ΔX_c).

Various authors report different melting points for the different crystalline phases of PVDF films[13,37,38]. For example, M. Benz and W. B. Euler[37] report following results: for predominantly α-phase, T_m = 157.9±0.6 ^oC, for pure as-cast γ phase, T_m = 161.3±0.9 ^oC, and for stretched, predominantly β-phase, T_m = 160-161 ^oC. These values vary greatly within the authors and to make a strict estimation of what the T_m for each crystalline phase should be is very difficult, since the T_m depends strongly on the resin used, polymerization condition, and also on lamellae thickness[13,38]. Small lamellae thickness reason low onset melting temperatures in PVDF[38].

The degree of crystallinity (ΔXc) of the samples was calculated by equation:

$$\Delta X_c = \frac{\Delta H_f}{\Delta H_{100}}$$

where ΔH_f is the melting enthalpy or heat of fusion of the composite and ΔH_{100} is the melting enthalpy for a 100% crystalline sample of pure PVDF[5].

In various articles is reported that ΔH_{100} for pure α- and γ- or β phases are not known, and ΔH_{100} is taken as the melting temperature of totally crystalline material (ΔH_{100} = 104.5 J/g)[37-39]. In this work ΔH_{100} was taken 103.4 J/g, according to D. Miranda et al. this value corresponds to β-phase[5].

Figure 4.26 summarizes the thermal data collected by DSC for PVDF/Cu nanospheres. The evolution of the melting temperature (T_m), degree of crystallization (ΔX_c) for both pressed and unpressed samples are depicted. Table 4.5 contains the computed thermal data to facilitate interpretation.

ΔX_c for unpressed samples decreases when spherical Cu nanoparticles were added (Table 4.5). Unpressed samples do not exhibit major changes between them (taking into account also the measurement error) with increasing Cu spheres content.

On the other hand, T_m of unpressed sample does not change significantly: the crystalline lamellae thickness is not affected by adding Cu nanospheres to polymeric matrix.

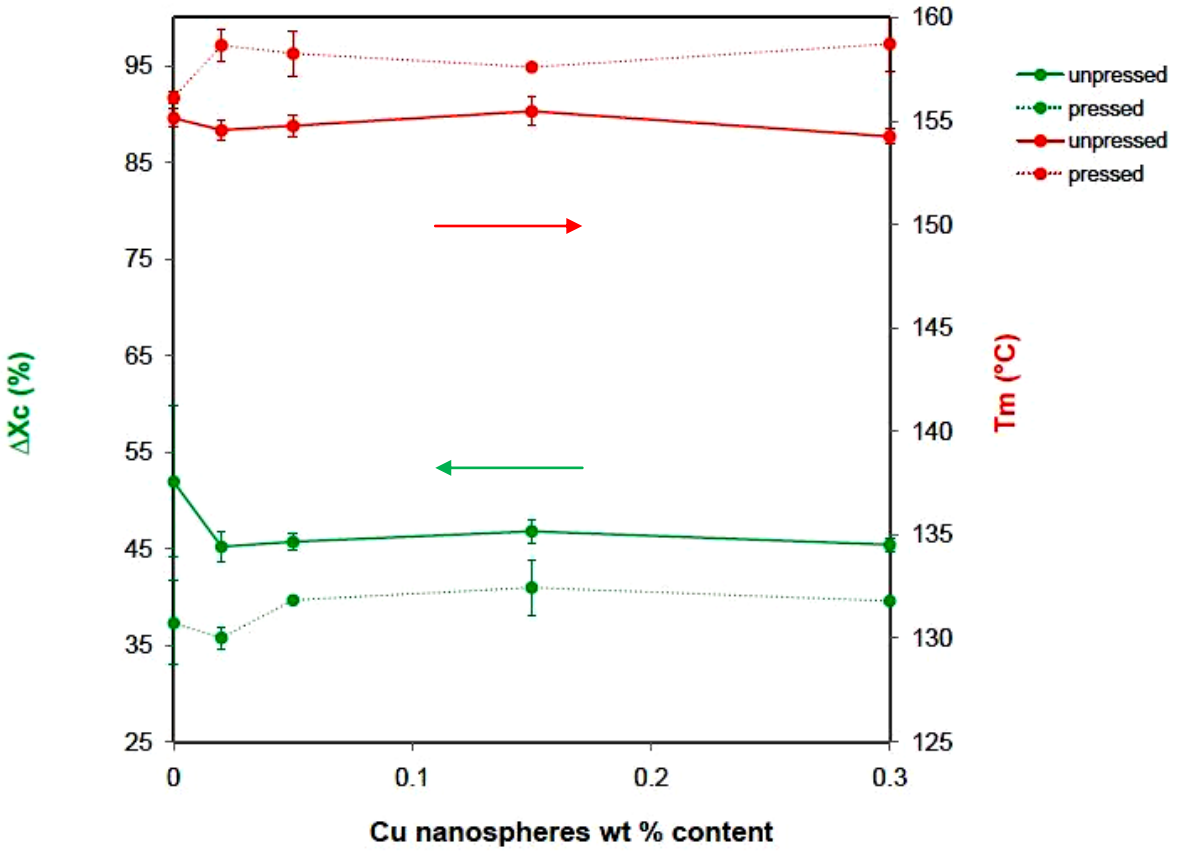

Figure 4.26 Degree of crystallinity (green) and melting temperature (red) for unpressed (solid line) and pressed (dot line) of PVDF/Cu nanospheres composites with different Cu content. The error bars are marked in the figure.

The crystallinity of pressed sample decreases considerably in relation to the unpressed ones, but a slightly increase in ΔX_c is noted with the increase in the Cu content (Table 4.5).

T_m of pressed sample increases compared to unpressed ones, meaning that during hot pressing the morpholgy of the polymer was affected resulting in thicker crystalline lamellaes. Interestingly there is a slight increase of imbedded polymer T_m relative to the pure PVDF. Therefore, T_m is in close relation with polymer morphology.

Lower ΔH_f and ΔX_c for pressed samples may be related to better packing of PVDF chains.

Table 4.5 Compiled results for melting temperature (T_m), heat of fusion (ΔH_f), and degree of crystallinity (ΔX_c) measured by DSC for PVDF/Cu nanospheres pressed (p.) and unpressed (unp.) samples.

Sample	T_m (^oC)		ΔH_f (J/g)		ΔX_c (%)	
	p.	unp.	p.	unp.	p.	unp.
PVDF	156.1±0.3	155.1±0.5	37.2±2.6	51.0±5.4	37.3±4.3	51.9±7.8
PVDF-0.02CuSph	158.6±0.8	154.5±0.5	36.9±1.1	46.7±1.7	35.7±1.1	45.2±1.6
PVDF-0.05CuSph	158.2±1.1	154.7±0.5	41.0±0.1	47.3±0.9	39.7±0.1	45.7±0.9
PVDF-0.15CuSph	157.6±0.1	155.4±0.7	42.3±3.0	48.4±1.3	40.9±2.9	46.8±1.2
PVDF-0.30CuSph	158.7±1.3	154.2±0.4	40.9±0.1	46.9±0.7	39.5±0.1	45.4±0.7

Figure 4.27 illustrates thermal properties of PVDF/Cu nanowires. First to notice, there are two trends similar to PVDF/Cu nanospheres composites: ΔX_c of pressed samples is smaller than ΔX_c of unpressed samples and T_m of pressed samples is higher compared to T_m of unpressed samples. Therefore, in both cases during hot pressing thicker crystalline lamellae are formed but the overall crystallinity is reduced (Tab. 4.6).

Related to ΔX_c of both pressed and unpressed samples, the tendency is different than the one noticed in the case of PVDF/Cu nanospheres. The polymer imbedded with nanoparticles displays a higher ΔX_c than pure polymer (Fig. 4.27), although it is worth to consider that the error of measurement is quite high. It seems that polymeric films do not have an homogenous morphology. The addition of nanoparticles increases the crystallization degree of the polymer matrix compared to pure PVDF, except for PVDF-0.30CuNw in the case of unpressed samples. In case of pressed samples, the highest value is found for PVDF-0.15CuNw (48.3 %), for which the spherulites size is also the highest (Fig. 4.11). Meanwhile ΔX_c of both pressed and unpressed sample for PVFD/Cu nanowires increases in comparison with ΔX_c of pure PVDF, where there is no increase of ΔX_c with increase of Cu nanowires content.

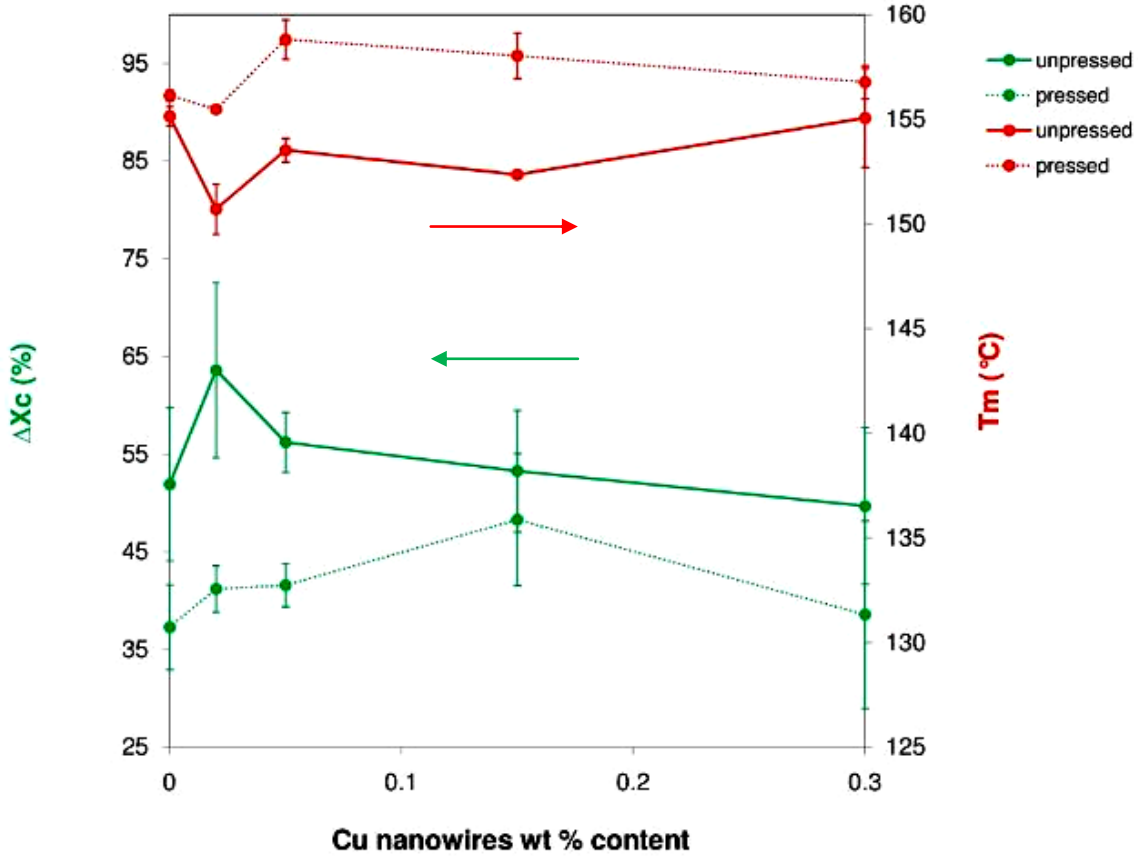

Figure 4.27 Degree of crystallinity (green) and melting temperature (red) for unpressed (solid line) and pressed (dot line) of PVDF/Cu nanowires composites with different Cu content. The error bars are marked in the figure.

Table 4.6 lists the computed thermal results.

Table 4.6 Compiled results for melting temperature (Tm), heat of fusion (ΔHf), and degree of crystallinity (ΔXc) measured by DSC for PVDF/Cu nanowires pressed (p.) and unpressed (unp.) samples.

Sample	T_m (°C)		ΔH_f (J/g)		ΔX_c (%)	
	p.	unp.	p.	unp.	p.	unp.
PVDF	156.1±0.3	155.1±0.5	37.2±2.6	51.0±5.4	37.3±4.3	51.9±7.8
PVDF-0.02CuNw	155.4±0.1	150.7±1.2	41.2±0.4	62.7±11.9	41.2±2.4	63.6±8.9
PVDF-0.05CuNw	158.8±0.9	153.5±0.6	41.7±4.2	55.3±0.4	41.5±2.2	56.2±3.1
PVDF-0.15CuNw	158.0±1.1	152.3±0.1	48.2±4.5	52.4±3.7	48.3±6.7	53.3±6.2
PVDF-0.30CuNw	156.7±0.8	155.0±2.4	39.9±9.9	50.4±8.3	38.6±9.6	49.7±8.0

Based on DSC results it can be stated that both PVDF/Cu nanospheres and PVDF/Cu nanowires composites crystallizes in spherulites which contain thin crystalline lamellae, since melting temperature is low (around 155-158 ^{o}C). This goes in agreement with the affirmation expressed in Ref. 3 that lamellae thickness depends on solution crystallization temperature, at lower temperatures, thinner crystalline lamellae are obtained.

Further, nanowires Cu particles when imbedded into the polymer increase the degree of crystallinity, while nanospheres diminish it. This phenomenon may be related with particles agglomeration, which is higher in case of nanospheres.

4.2.1 Partial conclusions

There are several conclusions to be drawn regarding the microstructural and morphological analysis of the composites prepared in this work :

- after hot pressing, the porosity was successfully eliminated from the nanocomposites films.

- the polymeric matrix consists largely of γ-phase, with low content in α-phase, and traces of β-phase. The inclusion of nanoparticles in different amounts, with different dimensionality and shape has no relevant effect on the phase in which PVDF crystallizes. Pressed and unpressed samples consist also of same phases.

- LSPR bands in UV-Vis spectra appear only for PVDF/Cu samples high in Cu content. XRD patterns show characteristic Cu signals only in the case of PVDF-0.30CuNw. As expected, Cu nanowires are more stable to oxidation than Cu spheres.

- PVDF matrix crystallizes in spherulitic structure regardless of the content, dimensionality and shape of Cu nanoparticles.

- Cu nanoparticles are randomly distributed in the PVDF matrix. Spherical particles tend to agglomerate more, while nanowires occur mostly individually and with no preferred orientation.

- Cu nanospheres promote the formation of smaller spherulites when increasing Cu content, whereas Cu nanowires induce the formation of larger crystallites.

- The melting temperatures for both PVDF/Cu nanospheres and PVDF/Cu nanowires is rather low (155-158 ^{o}C) indicating the formation of thin crystalline lamellae in polymeric matrix. Hot pressing diminishes the degree of crystallinity of the films, but increases the melting temperature. In the case of PVDF/Cu nanospheres, the addition of Cu spherical particles depresses the formation of nucleation sites, while in PVDF/Cu nanowires the addition of Cu nanowire particles promotes a higher crystallinity compared to pure PVDF.

4.3 Electrical and thermal conductivity properties analysis

The main scope of this work is to produce polymeric composites with high dielectric constant and thermal conductivity, therefore the assessment of these properties is fundamental. The electrical and thermal conductivity measurements results are presented and discussed in this chapter.

4.3.1 Electrical measurements

Figure 4.28 illustrates the dielectric constant and dielectric loss as a function of frequency and Cu content for PVDF/Cu nanospheres composites.

The highest found reported values of dielectric constant of PVDF/metallic fillers nanocomposites is of 3800 (10^2 Hz) at 23 vol% (corresponds to percolation threshold) of $Al_{65}Cu_{23}Fe_{12}$.[3] Regarding the use of small metallic fillers contents close to ones used in this work, a dielectric constant of 26.7 (10^3 Hz) for 0.02 wt% Ag loading in a PVDF β-phase matrix is reported[5].

It can be seen that the addition of Cu spheres raises the dielectric constant (ε') of the composites (from 12.5 of pure PVDF to 19.9 for PVDF-0.30CuSph). The increase of ε' can be understood as stated earlier accordingly to "Boundary layer capacitor effect" and "Maxwell-Wagner-Sillar interfacial polarization". "Boundary layer capacitor effect" treats the nanocomposites as equivalent elementary capacitors, where metallic fillers particles or clusters are isolated by thin dielectric insulator layer and can act as electrodes when an external electrical field is applied, which gives rise to dielectric constant of the nanocomposites[1].

"Maxwell-Wagner-Sillar interfacial polarization" accounts the ε' increase on accumulation and blockage of charge carriers at the thin insulating boundary of the interface of the two components of the nanocomposite, resulting in polarization increase of the matrix[3].

The increase of ε' is quite large for inclusion of 0.02% of nanoparticles (from 12.5 to 17.5 at 10^3 Hz). For larger Cu content ε' increases gradually at a lower rate, reaching a value of 19.9 (10^3 Hz) for PVDF-0.30CuSph.

It can be noticed that the curves of dielectric constant of the nanocomposites do not show clear dispersion especially in low frequency range. This phenomenon may be attributed to the oxidation of Cu nanospheres.

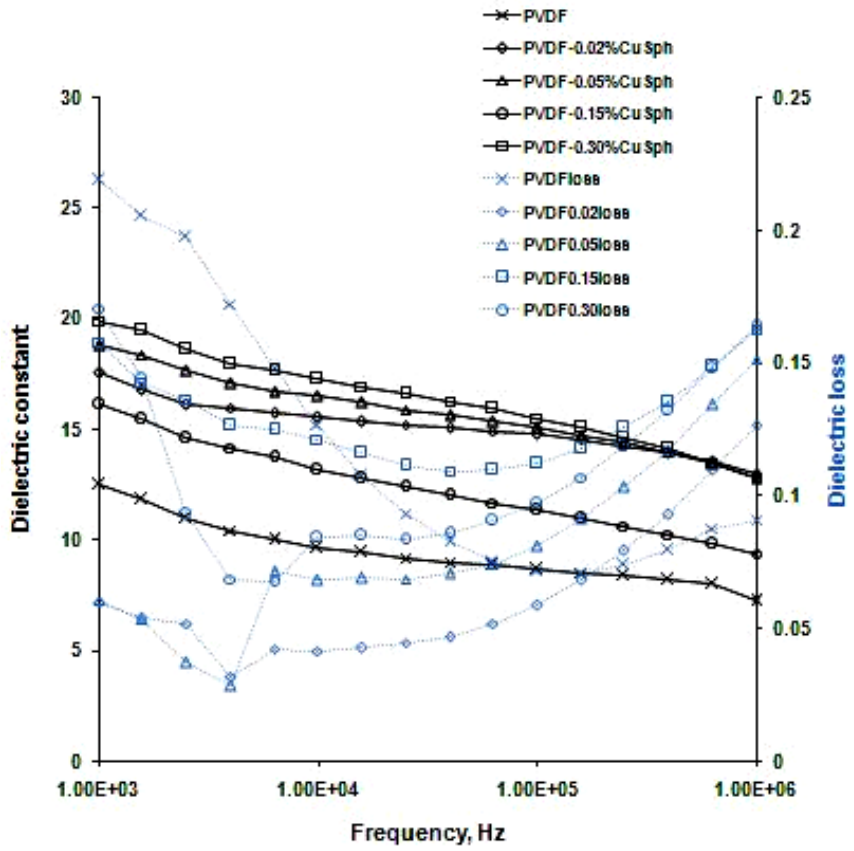

Figure 4.28 Dielectric constant and dielectric losses at room temperature for PVDF/Cu nanospheres composites with different Cu content.

Dielectric loss ($\tan\delta_e$) has a complicated evolution (Fig. 4.28). While at lower frequency, PVDF shows quite high $\tan\delta_e$ (0.23), the dielectric loss of nanocomposites is lower with no

apparent dependence of Cu nanospheres concentration. At higher values of frequencies the trend changes: PVDF shows a low $\tan\delta_e$ while the dielectric loss of nanocomposites increases.

Figure 4.29 shows the dielectric constant and loss at room temperature for PVDF/Cu nanowires composites with different Cu content.

The addition of Cu nanowires to the polymeric matrix results in a significant enhancement of ε' of the composites. For a concentration of 0.02 wt % Cu nanowires, ε' raises from 12.5 (pure PVDF) to 19.4. The highest values are obtained as expected for PVDF-0.30CuNw (24.4).

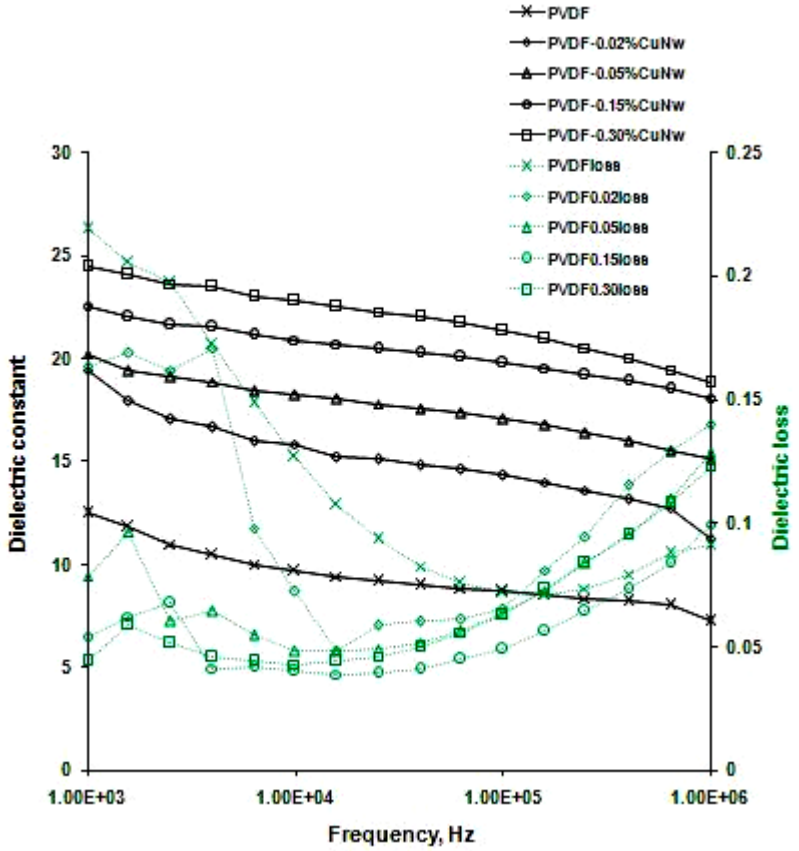

Figure 4.29 Dielectric constant and dielectric losses at room temperature for PVDF/Cu nanowires composites with different Cu content.

Dielectric constant shows a relevant increase with Cu nanowires content (Fig. 4.29) compared to PVDF/Cu nanospheres composites (Fig. 4.28). Moreover, the dielectric constants for same concentration of Cu, show higher values in case of Cu nanowires than Cu

nanospheres. Thus, nanowires Cu particle enhance more effectively the dielectric constant of the composite.

Curves of dielectric constant in function of frequency show a clear dispersion among them.

It is known that the dielectric constant of the polymer depends on its microstructure, phase content and degree of crystallinity[5]. Higher enhancement of ε' and clearer dispersion of curves for PVDF/Cu nanowires may be a contribution of several factors: the degree of crystallinity is generally higher as discussed before (for concentration of 0.02 wt % Cu, ΔX_c for nanowires raises from 35.7%, the value corresponding to nanospheres, to 41.2 %), anisotropy of Cu nanowires, and at last but not at least the fact that nanowires are more resistant to oxidation compared to nanospheres.

Dielectric loss of PVDF/Cu nanowires behaves similarly as PVDF/Cu nanospheres.

Evolution of dielectric constant as a function of Cu content for PVDF/Cu nanospheres is presented in Figure 4.31. It can be seen the general trend of ε' to increase with Cu nanospheres concentration, except sample PVDF-0.15CuSph. The measurement error increases with Cu content, indicating that by adding Cu nanoparticles, the particles are not homogeneously distributed among the film.

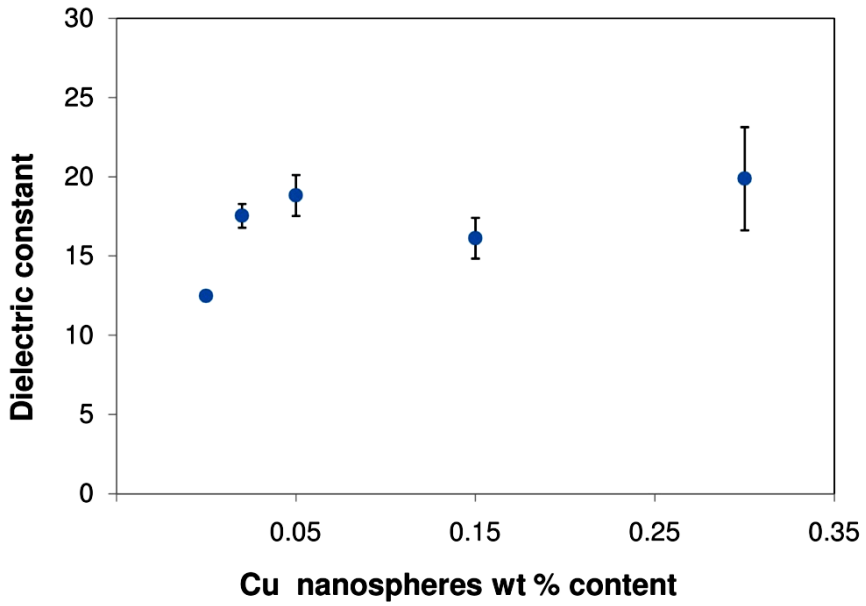

Figure 4.30 Evolution of dielectric constant as a function of Cu content for PVDF/Cu nanospheres composites at room temperature and 1 kHz.

Figure 4.31 shows the evolution of dielectric constant as a function of Cu content for PVDF/Cu nanowires.

Dielectric loss enhancement is greater compared to PVDF/Cu nanospheres and it increases notably with Cu nanowires content. Also, the measurement error is rather low, indicating that the nanoparticles were distributed more uniformly among the polymeric film.

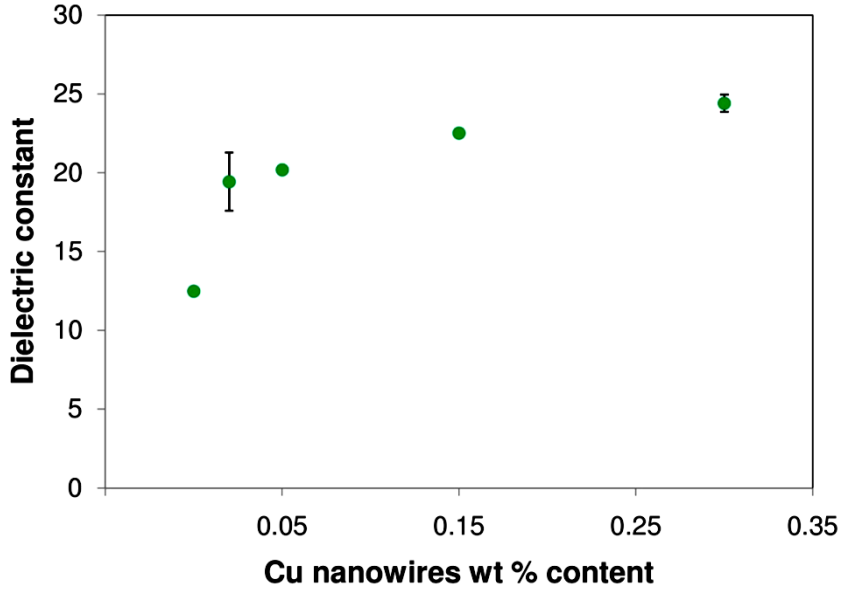

Figure 4.31 Evolution of dielectric constant as a function of Cu content for PVDF/Cu nanowires composites at room temperature and 1 kHz.

4.3.2 Thermal conductivity measurements

There is few data in literature dealing with PVDF composites thermal conductivity. A value of 0.55 $W \cdot m^{-1} \cdot K^{-1}$ in draw direction and 0.125 $W \cdot m^{-1} \cdot K^{-1}$ in transverse direction has been reported[10]. D. W.Chae et al. reports a value of 0.21 $W \cdot m^{-1} \cdot K^{-1}$ for pure PVDF[4], while X. Huang et al. obtains 0.24 $W \cdot m^{-1} \cdot K^{-1}$ [1]. The value obtained for pure PVDF in our case is 0.29 $W \cdot m^{-1} \cdot K^{-1}$.

The experimental thermal conductivities data displayed as function of weight Cu nanospheres content at room temperature are shown in Figure 4.32. It can be noticed that addition of Cu nanospheres is effective in improving thermal conductivity of PVDF matrix compared to the value of pure PVDF. A notable improvement of thermal conductivity occurs

at the loading level higher than 0.15 wt % and achieves 0.42 $W \cdot m^{-1} \cdot K^{-1}$ for 0.15 wt % and 0.39 $W \cdot m^{-1} \cdot K^{-1}$ for 0.30 wt %, which is nearly 1.4 times of pure PVDF.

Analyzing Figure 4.32, it can be seen that there is no strict increase of thermal conductivity with Cu content. For example, PVDF-0.30CuSph (0.39 $W \cdot m^{-1} \cdot K^{-1}$) shows slightly lower thermal conductivity than PVDF-0.15CuSph (0.42 $W \cdot m^{-1} \cdot K^{-1}$). This may be due interfacial thermal resistance of Cu oxides resulted from the oxidation

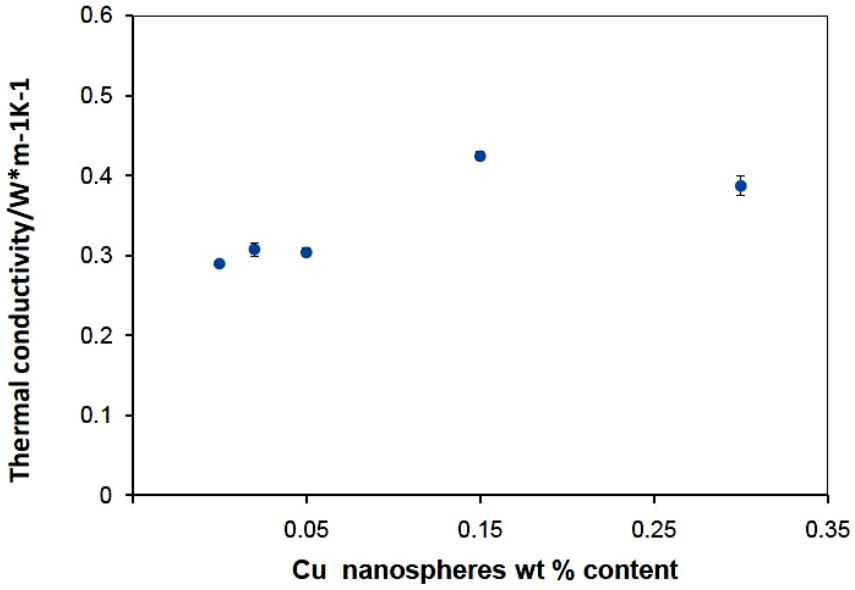

Figure 4.32 Thermal conductivity as a function of Cu content for PVDF/Cu nanospheres composites at room temperature.

Figure 4.33 displays thermal conductivity results for PVDF/Cu nanowires. Thermal conductivity improvement of PVDF/Cu nanowires is greater than those of PVDF/Cu nanospheres. There is a significant thermal conductivity enhancement starting with 0.05 wt % Cu nanowires loading (around 0.45 $W \cdot m^{-1} \cdot K^{-1}$). But after 0.05 wt % loading, there is no significant difference within the samples. Thermal conductivity of PVDF-0.30CuNw increases almost 1.6 times of pure PVDF.

As to our knowledge, maximum reported value of thermal conductivity of PVDF nanocomposites was 6.5 $W \cdot m^{-1} \cdot K^{-1}$ for 120 wt % filler in PVDF/Ag nanocomposite[1]. On the other hand, D. W. Chae et al.[4] reported only 0.38 $W \cdot m^{-1} \cdot K^{-1}$ for 90 wt % Ag loading, while D. Huang et al. [1] reports for same Ag content (90 wt %) a value of 1.25 $W \cdot m^{-1} \cdot K^{-1}$. Comparing

above mentioned data with results of this work, a rather high increase of thermal conductivity was obtained at very low Cu nanoparticles concentration. Further, PVDF/Cu nanowires display higher value of thermal conductivity than PVDF/Cu nanospheres most probably due to lower oxidation and anisotropy of Cu nanoparticles.

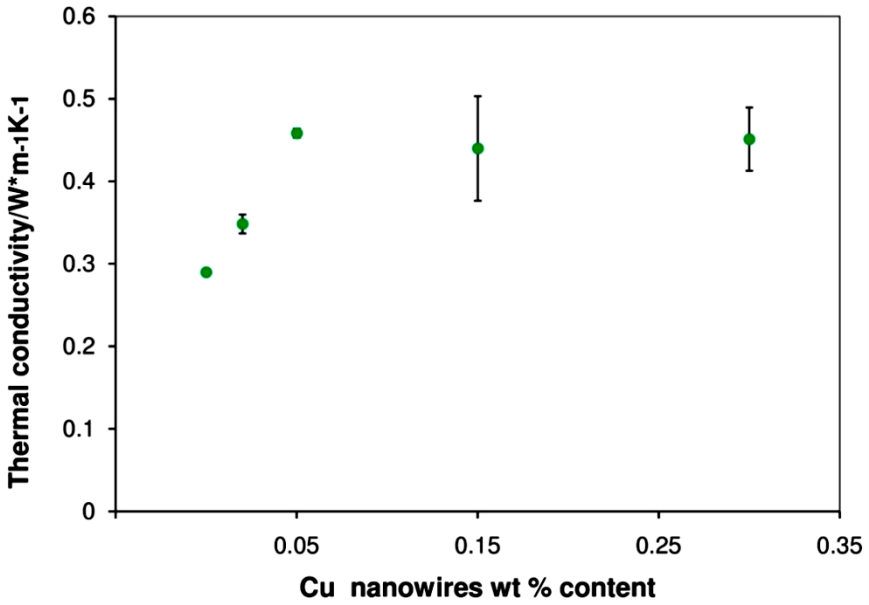

Figure 4.33 Thermal conductivity as a function of Cu content for PVDF/Cu nanowires composites at room temperature.

4.3.3 Partial conclusions

- The nanocomposites show enhancement in dielectric response with Cu nanoparticles addition. PVDF/Cu nanowires present a higher dielectric increase than PVDF/Cu nanospheres. The highest value of ε' at 10^3 Hz was 19.9 (1.6 times of pure PVDF) for PVDF/Cu nanospheres (0.30 wt %) and 24.4 (2 times of pure PVDF) for PVDF/Cu nanowires (0.30 wt %).

- A notable increase of thermal conductivity occurs when Cu nanoparticles are added. PVDF/Cu nanowires show higher values for thermal conductivity than PVDF/Cu nanospheres. The highest value of thermal conductivity was 0.42 $W \cdot m^{-1} \cdot K^{-1}$ (1.4 times of pure

PVDF) for PVDF/Cu nanospheres (0.15 wt %) and 0.45 (1.6 times of pure PVDF) for PVDF/Cu nanowires (0.30 wt %).

- The higher enhancement in dielectric and thermal conductivity response for PVDF/Cu nanowires may be due to better resistance to oxidation and anisotropy of Cu nanowires particles.

5. Conclusion

Finally, the major results of the present work are illustrated in Table 5.1.

Table 5.1 Literature collected results at room temperature on dielectric and thermal conductivity properties of PVDF/ various fillers nanocomposites with present work contribution added.

PVDF with	Filler concentration	Phase	Properties				Reference
			Dielectric constant	Increase %	Thermal Conductivity (W/mK)	Increase %	
Pure	0	α	8.3 (10^3 Hz)	-	-	-	5
Pure	0	β	12.3 (10^3 Hz)	-	-	-	5
Pure	0	γ	-	-	-	-	
Ag	15.3 vol%	α	NR	NR	0.38	81	4
Ag	20 vol%	NR	120 (10^3 Hz)	1544	6.5	2608	1
Ag	0.02 wt%	α	14.1 (10^3 Hz)	41.1	NR	NR	5
Ag	0.02 wt%	α (30%) & β (70%)	26.7 (10^3 Hz)	54	NR	NR	5
Ni	5* vol%	NR	112 (10^3 Hz)	1020	NR	NR	14
Ni	28* vol%	NR	2050 (10^2 Hz)	20400	NR	NR	2
Ni	20 vol%	NR	68 (10^4 Hz)	548	NR	NR	6
$Al_{65}Cu_{23}Fe_{12}$	23*vol%	NR	3800 (10^2 Hz)	34445	NR	NR	3
Cu spherical	0.30 wt%	γ	19.9 (10^3 Hz)	59	0.39	34	This work
Cu nanowires	0.30 wt%	γ	24.4 (10^3 Hz)	95	0.45	55	This work

NR= not reported

* particle volume fraction corresponding to percolation threshold.

Nanocomposites with high dielectric constant and high thermal conductivity were prepared with low Cu nanoparticles concentration far below the percolation threshold. This makes PVDF/Cu nanocomposites a promising candidate for microelectronics and high-voltage industries.

6. Future work

Future work should be focused mainly on the following aspects:

- Monitoring of Cu oxidation in PVDF matrix. Finding a suitable method to prevent Cu oxidation within the polymer. Methods like encapsulation of Cu nanoparticles in Ag layer should be considered.

- Incorporation of larger copper nanoparticles amounts in order to reach percolation threshold. Identification of the role of dimensionality (shape and size) on this limit.

- Controlling the copper nanoparticles agglomeration and orientation in the polymer matrix.

- Tailoring the nanocomposites preparation so that electroactive β-phase is obtained in the polymer matrix.

- Incorporation of other metal fillers like Ag, Ni should be also considered.

References

[1] Huang X., Jiang P., Xie L. Applied Physics Letters 95, 242901 (2009).
[2] Panda M., Srinivas V., Thakur A. K. Applied Physical Letters 92, 132905 (2008).
[3] Venkatesh Ch., Srinivas V., Panda M., Rao V. V. Solid State Communications 150 (2010) 893-896.
[4] Chae, D. W., Hwang, S. S., Hong S. M., Hong S. P. (2007). Mol. Cryst. Liq. Cryst., 464, 233
[5] Miranda, D., Sencadas, V., Sanchez-Iglesias, A., Pastoriza-Santos, I., Liz-Marzan, L. M., Gomez Ribelles, J. L., Lanceros-Mendez, S.(2008). J. Nanosci. Nanotechnol. 9, 1-7
[6] Xu, H.P., Dang, Z. M., Bing, N. C., Wu, Y. H., Yang, D. D. (2010). J. Appl. Phys., 107, 034105.
[7] Shackelford J. F., Alexander W. Materials Science and Engineering handbook, CRC Press LLC (2001).
[8] Tashiro K. Crystal structure and phase transition of PVDF and related copolymers, In: Nalwa HS, editor. Ferroelectric polymers. New York: Marcel Dekker: 1995.
[9] http://en.wikipedia.org/wiki/Pvdf (retrieved on 22.06.11).
[10] Chilton J. A., Goosey M. T. Special polymers for electronics and optoelectronics, 1995 Chapman & Hall.
[11] Park Y. J., Kang Y. S., Park C. European Polymer Journal 41 (2005) 1002-1012.
[12] Lovinger A. J. Macromolecules 1981, 14, 322-325.
[13] Gregorio R. Journal of Applied Polymer Science 100 (2006) 3272-3279.
[14] Li, W.,Yu, L., Zhu, Y., Hua, D. (2010). J. Phys. Chem. 114, 14004-14007
[15] Diaz-Droguett D. E., Espinoza R., Fuenzalida V. M. Applied Surface Science 25 (2011) 4597-4602.
[16] Pastoriza-Santos I., Sánchez-Iglesias A., Rodríguez-González B., Liz-Marzán L. small 2009, 5, No. 4, 440-443.
[17] Lisiecki I., Pileni M. P. J. Am. Chem. Soc. 1993, 115, 3887.
[18] Pedersen D. B., Wang S., Liang S. H. J. Phys. Chem. C 2008, 112, 8819.
[19] Cho Y-S., Huh Y-D. Materials Letters 63-2 (2009) 227-229.
[20] Rao C.N.R., Deepak F.L., Gundiah G., Govindaraj A. Progress in Solid State Chemistry 31 (2003) 5–147.
[21] Leng Y. Materials characterization: Introduction to microscopic and spectroscopic methods.
[22] Hesse M., Meier H., Zeeh B. Spectroscopic Methods in Organic Chemistry 2008 Georg Thieme Verlag, Stuttgart.
[23] Bormashenko Ye., Pogreb R., Stanevsky O., Bormashenko Ed. Polymer Testing 23 (2004) 791-796.
[24] Gregorio R., Borges D. S. Polymer 49 (2008) 4009-4016.
[25] Boccaccio T., Bottino A., Capannelli G., Piaggio P., Journal of Membrane Science 210 (2002) 315-329.
[26] E. Smith, G. Dent “Modern Raman Spectroscopy” 2005.
[27] Martinelli A., Matic A., Jacobsson P., Börjesson, Navarra M. A., Munaò D., Panero S., Scrosati B. Solid State Ionics 178 (2007) 527-531.
[28] Silva M.P., Sencadas V., Botelho G., Machado A. V., Rolo A. G., Rocha J. G., Lanceros-Mendez S. Materials Chemistry and Physics 122 (2010) 87-92.

[29] Thomas M., Ultraviolet and Visible Spectroscopy, second edition, published on behalf of ACOL, 1996.
[30] Liz-Marzan L. M., Langmuir 2006, 22, 32-41.
[31] Park S. Y., Chae H. K., Chem. Mater. 2010, 22, 6280-6290.
[32] Ung T., Liz-Marzan L. M., Mulvaney P., Colloids and Surfaces A: Physicochemical and Engineering Aspects 202 (2002) 119-126.
[33] http://www.mrl.ucsb.edu/mrl/centralfacilities/xray/xray-basics/index.html (retrieved on 13.07.2011)
[34] Dikshit, A., Nandi, A. Macromolecules, 33, 2616 (2000).
[35] Manna S., Batabyal S. K., Nandi A. K. J. Phys. Chem. B 2006, 110, 12318-12326.
[36] http://www.ietltd.com/pdf_datasheets/DSC%2050%20Data%20Sheet.pdf (retrieved on 13.07.2011).
[37] Benz M.,Euler W. B. Journal of Applied Polymer Science 89 (2003) 1093-1100.
[38] Zhao X., Cheng J., Chen S., Zhang J., Wang X. Journal of Polymer Science: Part B: Polymer Physics 48 (2010) 575-581.
[39] Lanceros-Méndez S., Mano J. F., Costa A. M., Schmidt V. H. J. Macromol. Sci.-Physics, B40(3&4), 517-527 (2001).
[40] Gubler U., Raunhardt M., Stump A. Thin Solid Films 515 (2006) 1737-1740.
[41] TCi Operator Manual X130041 Rev. B.
[41] http://www.ctherm.com/products/tci_thermal_conductivity/how_the_tci_works/ (retrieved on 14.06.11)
[42] Chang Y., Lye L. M., Zeng C. H. Langmuir 2005, 21, 3746-3748.
[43] Zhang X., Zhang D., Ni X., Zheng H. Solid State Communication 139 (2006) 412-414.
[44] Hylar 9009 ASTM technical data sheet.
[45] Callister W. D. Materials Science and Engineering: an Introduction-5th ed., John Wiley & Sons, Inc (2000).
[46] Vitor João Gomes da Silva Sencadas Influência das condições de processamento na morfologia e fases cristalinas do PVDF e nas transições de fase do copolímero P(VDF-TrFE), Universidade do Minho, Julho de 2005.
[47] Y.S. Touloukian, R.W. Powell, C.Y. Ho, P.G. Klemens, Thermophysical Properties of Matter, vol. 2, Thermal Conductivity: Nonmetallic Solids, IFI/Plenum Press, New York, 1970.
[48] He Y. Thermochimica Acta 419 (2004) 135-141.
[49] Electrical insulating materials and their application, by R. W. Sillars. Peter Peregrinus Ltd. 1974.
[50] http://www.patsnap.com/patents/view/US4053702.html
[51] Gualous, H., Louahlia-Gualous, H., Gallay, R., Miraoui, A. Industry Applications 45 (2009) 1035-1044.
[52] http://goldbook.iupac.org/G02593.html
[53] http://goldbook.iupac.org/T06406.html
[54] http://goldbook.iupac.org/T06435.html
[55] http://plc.cwru.edu/tutorial/enhanced/files/polymers/struct/struct.htm (retrieved on 18.07.11).
[56] Balandin, A. A. et al. (2008-02-20). "Superior Thermal Conductivity of Single-Layer Graphene". Nano Letters ASAP 8 (3): 902–907.

[57] Frank, I. W., Tanenbaum, D. M., Van Der Zande, A.M., and McEuen, P. L. (2007). "Mechanical properties of suspended graphene sheets". J. Vac. Sci. Technol. B 25 (6): 2558–2561. Bibcode 2007JVSTB..25.2558F. doi:10.1116/1.2789446
[58] http://www.asiinstr.com/technical/Dielectric%20Constants.htm#Section (retrieved on 21.07.11)
[59] J.MEMS,DEC 1995,Vol.4,NO.4, p.234
[60] IEEE 5th International Symposium on Micro Machine and Human Science proceedings,Nagoya, Oct 1994, p.75
[61] http://ndeaa.jpl.nasa.gov/ndeaa-pub/USDC/IEEE-01-rsntor-chrctr.pdf
[62] Horiuchi S., Tokura Y. Nature Materials 7 (2008) 357-366
[63] P. M. Vilarinho et al (eds), Scanning Probe Microscopy: Characterization, Nanofabrication and Device Application of Functional Materials, 3-33, 2005 Kluwer Academic Publishers, Printed in the Netherlands.
[64] Dang Z.-M., Nan C.-W. Ceramics International 31(2005) 349-351.
[65] Zhang X., Zhang D., Ni X., Zheng H. Solid State Communications 139 (2006) 412-414.